nature neuroscience

Betaine acts on a ligand-gated ion channel in the nervous system of the nematode *C. elegans*

Aude S Peden[1], Patrick Mac[1,7], You-Jun Fei[2,7], Cecilia Castro[3,4], Guoliang Jiang[2], Kenneth J Murfitt[3,5], Eric A Miska[3,5], Julian L Griffin[3,4,6], Vadivel Ganapathy[2] & Erik M Jorgensen[1]

Prior to the advent of synthetic nematocides, natural products such as seaweed were used to control nematode infestations. The nematocidal agent in seaweed is betaine, an amino acid that functions as an osmolyte and methyl donor. However, the molecular mechanisms of betaine toxicity are unknown. We identified the betaine transporter SNF-3 and the betaine receptor ACR-23 in the nematode *C. elegans*. Mutating *snf-3* in a sensitized background caused the worms to be hypercontracted and paralyzed, presumably as a result of excess extracellular betaine. These behavioral defects were suppressed by mutations in *acr-23*, which encodes a ligand-gated cation channel of the cys-loop family. ACR-23 was activated by betaine and functioned in the mechanosensory neurons to maintain basal levels of locomotion. However, overactivation of the receptor by excess betaine or by the allosteric modulator monepantel resulted in hypercontraction and death of the nematode. Thus, monepantel targets a betaine signaling pathway in nematodes.

Humans have long competed with parasitic nematodes for crops, livestock and personal health. Early farmers dealt with nematode infestations by using natural pesticides such as wormwood, tobacco and algae (seaweed), which contain natural phytochemicals that interfere with parasitic nematode development[1–3]. Seaweed extracts are rich in betaines (δ-aminovaleric betaine, γ-amino-butyric betaine and glycine betaine), and direct application of individual betaines to plants suppresses nematode growth as effectively as algal extract[4].

Glycine betaine, or simply 'betaine', is a ubiquitous non-canonical amino acid that acts as an osmolyte or as a methyl donor. In addition to its role in metabolism, betaine may have specific roles in the mammalian nervous system. Betaine has anti-epileptic properties[5–7] and the transporter BGT-1 is localized to dendritic spines and astrocytes in the mammalian brain[8].

In nematodes, betaine arrests larval development[2–4], but the molecular target of betaine is not known. The targets of synthetic anthelmintics are often ligand-gated ion channels. The imidazothiazoles directly activate acetylcholine-gated ion channels, which stimulates muscle contraction and paralyzes the worm[9,10]. The macrocyclic lactones open glutamate-gated chloride channels and inhibit pharyngeal pumping[11–13]. Amino-acetonitrile derivatives (AADs) are a recently discovered class of compounds that target a nematode-specific ion channel known as ACR-23 in *C. elegans*[14]. ACR-23 belongs to the nicotinic acetylcholine receptor subfamily, but its homolog in parasitic nematodes, MPTL-1, is not gated by acetylcholine or choline[15]. The endogenous ligand and biological function of ACR-23 remain to be characterized.

We studied the role of betaine in the nematode *C. elegans* and found that ACR-23 is a betaine receptor. First, we characterized the betaine transporter SNF-3 and observed that mutations in this transporter were subviable in a sensitized background lacking phospholipase Cβ. Second, mutations in *acr-23* suppressed this lethality, suggesting that excess betaine acts via ACR-23. Finally, ACR-23 was gated by betaine and potentiated by the AAD monepantel. Thus, ancient and modern anthelmintics act on the same target: a betaine-activated ion channel that is only found in nematodes.

RESULTS

An enhancer screen identifies a betaine transporter

We were able to identify the betaine pathway inadvertently while studying phospholipase Cβ function. In *C. elegans*, mutants lacking the only phospholipase Cβ gene (*egl-8*) exhibit subtle behavioral defects in locomotion and egg-laying, in contrast with the near lethal phenotype of mutants lacking Gαq, the upstream activator of phospholipase Cβ[16,17]. This modest loss-of-function phenotype in *egl-8* mutants suggests the existence of parallel pathways to inositol signaling that modulate locomotion. To uncover these pathways, we performed an F_2 enhancer screen in an *egl-8* mutant background. We screened 1,669 haploid genomes and identified a single mutation that caused a synthetic phenotype in the presence of an *egl-8* mutation. Mapping, rescue and sequencing experiments revealed that the enhancer was an allele of the *snf-3* gene (*sodium neurotransmitter symporter family-3*; **Supplementary Fig. 1a**). The *snf-3 egl-8* double mutants exhibited severe synthetic phenotypes (**Fig. 1a–d**): the strain

[1]Department of Biology and Howard Hughes Medical Institute, University of Utah, Utah, USA. [2]Department of Biochemistry and Molecular Biology, Georgia Regents University, Augusta, Georgia, USA. [3]Department of Biochemistry, University of Cambridge, Cambridge, UK. [4]Cambridge Systems Biology Centre, University of Cambridge, Cambridge, UK. [5]Wellcome Trust Cancer Research UK Gurdon Institute, University of Cambridge, Cambridge, UK. [6]The Medical Research Council Human Nutrition Research, Elsie Widdowson Laboratory, Cambridge, UK. [7]These authors contributed equally to this work. Correspondence should be addressed to E.M.J. (jorgensen@biology.utah.edu).

Received 9 July; accepted 11 October; published online 10 November 2013; corrected after print 5 December 2013; doi:10.1038/nn.3575

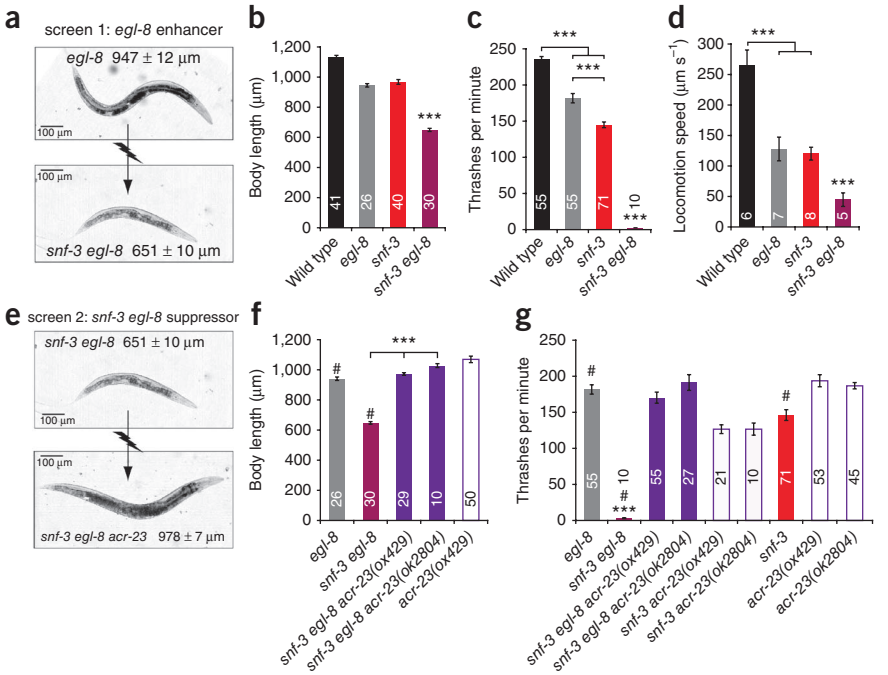

Figure 1 Two genetics screens reveal a betaine receptor. (**a**) *snf-3* was identified as an enhancer of the phosopholipase Cβ mutation *egl-8(sa47)*. Shown are images of an adult *egl-8(sa47)* mutant and an adult *snf-3(ox354) egl-8(sa47)* double mutant that were isolated in the screen. Mean lengths of 26 (*egl-8*) and 30 (*snf-3; egl-8*) adults are shown. (**b**) Hypercontracted phenotype. We plotted the mean body length of young adult worms. Error bars represent s.e.m. ***$P < 0.001$ relative to wild type and single mutants. (**c**) Quantification of locomotion in liquid using a thrashing assay. (**d**) Average locomotion speed over a 5-min period on an agar plate without food. Speed was determined using an automated worm tracking system. (**e**) *acr-23* was isolated as a suppressor of the *snf-3 egl-8* hypercontracted phenotype. Images of adult hermaphrodites of the *snf-3(ox354) egl-8(sa47)* double mutant ($n = 30$) and the *snf-3(ox354) egl-8(sa47) acr-23(ox429)* triple mutant ($n = 29$). (**f**,**g**) Quantification of the hypercontracted (**f**) and locomotion (**g**) phenotypes. Data represent the mean ± s.e.m. ***$P < 0.001$ compared to other mutants. For all histograms, the number of worms tested is shown inside each bar. Statistical significance was determined using one-way ANOVA followed by Tukey *post hoc* comparisons. # indicates data are the same as shown in **b** and **c**.

was subviable, uncoordinated and dumpy. The dumpy phenotype was a result of hypercontraction of the muscle, as it could be suppressed by mutations in the contractile apparatus *unc-22* (twitchin) and *unc-54* (myosin) (data not shown)[9]. The hypercontracted phenotype of *snf-3 egl-8* double mutants was fully synthetic: neither single mutant was hypercontracted (**Fig. 1a**,**b** and **Supplementary Fig. 1c**). The uncoordinated phenotype was also more severe than that of either single mutant (**Fig. 1c**,**d**). Multiple allelic combinations exhibited the same synthetic hypercontracted phenotype (data not shown), indicating that the phenotypes are not a result of background mutations.

snf-3 encodes a neurotransmitter transporter of the solute carrier 6 (SLC6) gene family. Members of this transporter family clear neurotransmitters from the synaptic cleft, including serotonin, dopamine, norepinephrine, GABA and glycine. SNF-3 is orthologous to the vertebrate betaine/GABA transporter (BGT1 or SLC6A12). Although we do not fully understand the genetic interaction between the betaine transporter and PLCβ, the synthetic phenotype provided a selection with which to identify the betaine receptor.

Hypercontraction in *snf-3 egl-8* is mediated by *acr-23*

Mutations in SLC6 transporters often result in constitutive signaling because the neurotransmitter cannot be cleared from the synaptic cleft[18,19]. For example, mice lacking the dopamine transporter are hyperactive[20], whereas worms lacking the same gene have defects in their locomotor behaviors[21,22]. These defects are consistent with the role of dopamine in the control of locomotion.

To determine whether the phenotype of *snf-3*, *egl-8* mutants is a result of constitutive betaine signaling, we screened for suppressors of the *snf-3* synthetic phenotype. Specifically, we mutagenized *snf-3 egl-8* double mutants with *N*-ethyl-*N*-nitrosourea (ENU) and screened for suppressors of the hypercontracted phenotype (**Fig. 1e**). We screened 37,000 haploid genomes and obtained 35 suppressors. The phenotypes of the triple mutants fell into three broad classes: those that resembled *egl-8* single mutants (*snf-3*–specific suppressors), those that resembled *snf-3* mutants (*egl-8*–specific suppressors) and those with new phenotypes.

The strongest *snf-3*–specific suppressor was the mutation *ox429*. We identified the suppressor mutation by genome resequencing and by transgenic rescue. o*x429* is an allele of the *acr-23* gene (*acetylcholine receptor like-23*) (**Supplementary Fig. 2a**). *acr-23* encodes a nematode-specific ligand-gated channel subunit and is predicted to function as a cation channel based on its sequence homology to acetylcholine receptors (**Supplementary Fig. 2c**). The only known function of ACR-23 is that it imparts sensitivity to the new class of anthelmintic drugs known as AADs. Genetic screens for AAD resistance in *C. elegans* identified 27 independent mutations in a single target, *acr-23* (ref. 14), and mutations in related receptor subunits in the same subfamily do not confer resistance to AAD[23].

acr-23(ox429) fully suppressed the hypercontracted (**Fig. 1f**) and uncoordinated phenotypes (**Fig. 1g**) of the *snf-3 egl-8* double mutants. For example, the double mutants were completely paralyzed in liquid (0% of wild-type rate; **Fig. 1g**), whereas the *snf-3 egl-8 acr-23* triple mutants thrashed actively (45% of wild-type rate; **Fig. 1g**). A deletion allele, *acr-23*(*ok2804*), also suppressed the double mutants (**Fig. 1f**–**g**). The triple mutants still exhibited *egl-8* phenotypes, including lethargy (**Fig. 1g**), constipation (data not shown) and a mild egg-laying defect (data not shown), suggesting that *acr-23* mutations specifically suppress *snf-3*, but not *egl-8*, pathways.

SNF-3 is a Na^+/Cl^--dependent betaine transporter

The vertebrate ortholog of SNF-3, betaine/GABA transporter 1 (BGT1 or SLC6A12), has two substrates, betaine and GABA. However, it has a higher affinity for GABA (K_m = 93 µM) than for betaine (K_m = 398 µM)[24,25]. In contrast, we found that SNF-3 transported betaine, but not GABA. Betaine is a noncanonical amino acid that is present in all organisms (**Fig. 2a**). It acts as an osmolyte to maintain cell volume during stress[26] and as a methyl donor in the conversion of homocysteine to methionine. Betaine is acquired either by dietary uptake using a plasma membrane transporter or is generated as an oxidation product of choline[27]. Ultimately, betaine is metabolized to glycine.

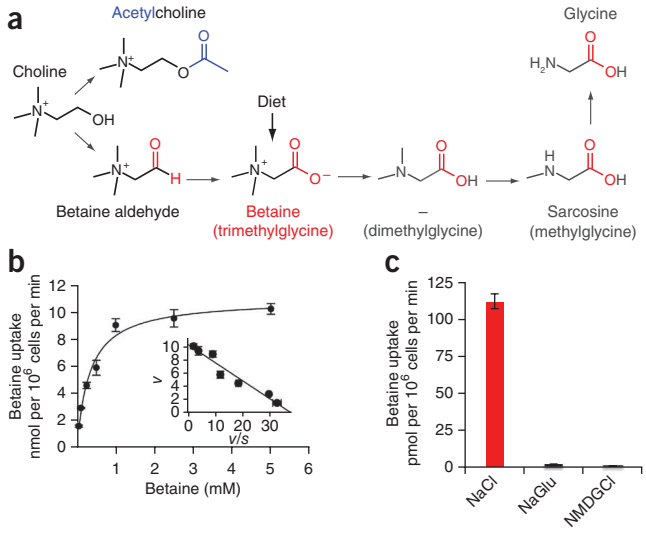

Figure 2 SNF-3 is a NaCl-dependent betaine transporter. (**a**) Betaine synthesis pathway. Betaine (*N*,*N*,*N*-trimethylglycine) is either acquired via diet or generated in two steps by oxidation of choline. (**b**) Saturation curve of betaine uptake by SNF-3 in HRPE cells. Error bars represent s.e.m. Each experiment was performed in triplicate. Inset, Eadie-Hofstee conversion of the same saturation data (*v*/*s*; betaine uptake velocity (*v*) versus betaine uptake velocity/betaine concentration (*v*/*s*)). K_m was calculated using the Eadie-Hofstee equation. (**c**) SNF-3–mediated uptake of betaine was dependent on Na^+ and Cl^- ions. HRPE cells were incubated with 2.5 µM betaine for 15 min in assay buffer containing either NaCl, NaGlu or NMDGCl. Gluconate replaced chloride ions (NaGlu) and sodium ions were replaced by NMDG-Cl. Error bars represent s.e.m. Each experiment was performed in triplicate.

To rapidly screen for the relevant substrate, we expressed SNF-3 in *Xenopus* oocytes and applied potential transport molecules. SLC6 transporters co-transport ions along with substrate molecules and are therefore electrogenic. We tested candidate substrates and found that only betaine induced a specific current (**Supplementary Fig. 3a**). GABA, the betaine metabolites dimethylglycine, *N*-methylglycine and glycine, and other related compounds are not substrates of the SNF-3 transporter.

To characterize the transport kinetics of SNF-3, we measured the accumulation of radio-labeled betaine in human retinal pigment epithelial (HRPE) cells, which do not express an endogenous betaine transporter. The expression of SNF-3 increased betaine uptake by more than 100-fold (108 ± 3 pmol per 10^6 cells per min) over control cells (0.8 ± 0.1 pmol per 10^6 cells per min). SNF-3–mediated transport was saturable with a K_m of 320 ± 50 µM (**Fig. 2b**); this value is similar to the affinity of BGT-1 for betaine (398 µM)[24]. As expected for protein-mediated transport, activity was saturable over a range of concentrations (**Fig. 2b** and **Supplementary Fig. 3b**) and voltages (**Supplementary Fig. 3c**). Similar to other SLC6 transporters, SNF-3 requires sodium and chloride to move substrates into cells against their chemical gradient. The absence of sodium (in *N*-methyl-D-glucamine (NMDG) chloride solution) or the absence of chloride (sodium gluconate solution) abolished betaine uptake (**Fig. 2c** and **Supplementary Fig. 3d**), and transport was voltage dependent (**Supplementary Fig. 3e**). The Michaelis constant of SNF-3 for sodium ($K_{0.5}^{Na}$) was 37 ± 1 mM with a Hill coefficient of 2.2 ± 0.1 (**Supplementary Fig. 3f**), and the corresponding value for chloride ($K_{0.5}^{Cl}$) was 12 ± 1 mM with a Hill coefficient of 1.0 ± 0.1 (**Supplementary Fig. 3g**). Thus, these data indicate that SNF-3 functions as a betaine transporter with a unidirectional influx of 1 betaine:2 Na^+:1 Cl^- per transport cycle.

In contrast with BGT1, SNF-3 did not transport GABA in our biochemical assays, and we observed this lack of GABA transport activity functionally. In the nematode, the GABA transporter is encoded by *snf-11* (ref. 28). Overexpression of the SNF-3 transporter is unable to compensate for the absence of the GABA transporter SNF-11 even when overexpressed under the *snf-11* promoter, indicating that SNF-3 cannot transport GABA *in vivo*[28]. The presence of a dedicated transporter suggests that betaine may have a specific role in cell signaling.

SNF-3 is required for betaine clearance

Members of the SLC6 transporter family clear neurotransmitters from synapses and the extrasynaptic space, thereby limiting their activity. To determine where SNF-3 functions, we examined *snf-3* expression using a functional *snf-3–GFP* transgene (**Supplementary Fig. 1b**). Transgenic worms displayed strong expression in the excretory canal, tail hypodermal cells, epidermis and vulval epithelia cells (**Fig. 3a**). SNF-3 was also expressed in some neurons, including the excretory canal–associated neuron (**Fig. 3a**), and some sensory neurons in the head including ILs, OLs, ADE and AQR (**Supplementary Fig. 2d**,**e**). We were able to rescue the hypercontraction and the locomotory phenotypes of *snf-3 egl-8* double mutants by expressing wild-type SNF-3 using the native *snf-3* promoter or using tissue-specific promoters for the excretory canal or skin (*glt-3* and *pdi-2* promoters, respectively; **Fig. 3b**). Notably, expressing SNF-3 in tissues that do not normally express the gene, such as the intestine, chemosensory neurons or acetylcholine motor neurons, also rescued the hypercontracted phenotype (**Fig. 3b**). Rescue required expression during larval development: expression of SNF-3 in the intestine during larval development (*vha-6* promoter), but not in the adult (*vit-2* promoter; **Fig. 3b**), rescued the hypercontracted phenotype. This stage-dependent rescue is consistent with the retarded larval development of *snf-3* mutants (**Supplementary Fig. 2e**). The non-cell autonomous rescue of the *snf-3 egl-8* phenotypes suggests that the hypercontracted and locomotory phenotypes are caused by a lack of betaine clearance; presumably any tissue, not just the epidermis and excretory canal, can remove the excess betaine.

In contrast with *snf-3*, *egl-8* was required in the nervous system, but not epidermis (**Fig. 3c**). Further analyses of EGL-8 revealed that the observed synthetic hypercontraction was a result of a defect in acetylcholine neurons (*unc-17* promoter). Expression in sensory neurons (data not shown) or in ventral cord motor neurons (data not shown) did not rescue the double-mutant phenotypes. Thus, the functional requirements for EGL-8 and SNF-3 are in separate tissues; the transporter SNF-3 functions primarily in the epidermis to clear betaine from the extracellular space, whereas EGL-8 is required in the nervous system to modulate neuronal activity.

Exogenous betaine paralyzes *snf-3* mutants

These data suggest that the phenotypes caused by *snf-3* mutants are a result of excess betaine in the extracellular space. If true, then high levels of exogenous betaine should mimic *snf-3* phenotypes. We grew *C. elegans* on different concentrations of betaine and tested their locomotion in liquid. Wild-type worms were not affected by 50 mM betaine (**Fig. 3d**). *egl-8* mutants were hypersensitive to 50 mM betaine and became sluggish in liquid, but they did not become hypercontracted. *snf-3* mutants were strongly hypersensitive to 50 mM betaine and were paralyzed in liquid. The toxic effect of betaine was mediated by ACR-23, as *snf-3 acr-23* double mutants were resistant to exogenous betaine (**Fig. 3d**). Wild-type worms grown at a higher

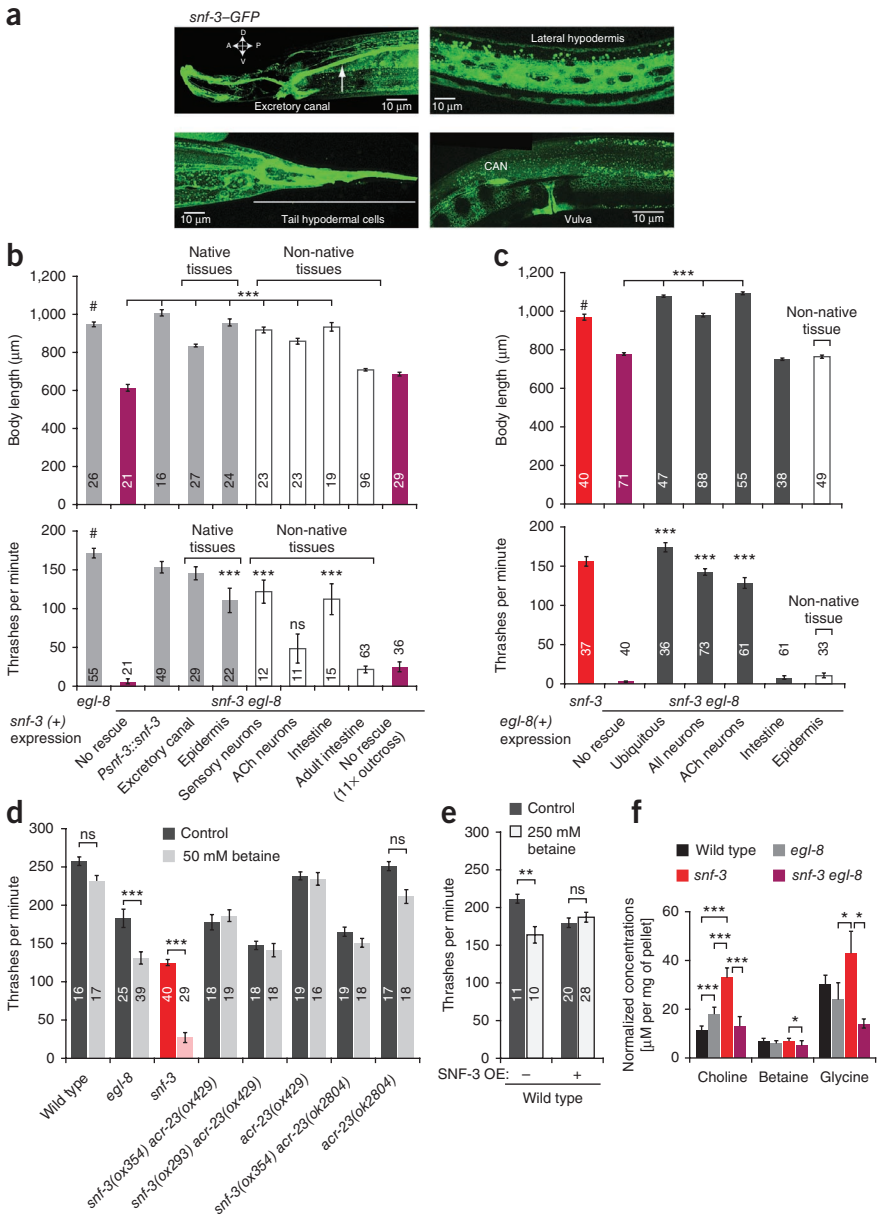

Figure 3 SNF-3 is required for betaine clearance. (**a**) Expression pattern of *snf-3–GFP*. Images show the head, tail, lateral midbody and vulva region of a transgenic hermaphrodite expressing GFP fused to genomic *snf-3* (P*snf-3*::*snf-3–GFP*::*snf-3* UTR). All images are of adult hermaphrodites; anterior is to the left. CAN, excretory canal–associated neuron. (**b**) *snf-3* tissue-specific rescue of the hypercontracted (above) and locomotion (below) phenotype. Top, expression of *snf-3* cDNA in excretory canal (*glt-3* promoter), skin (*pdi-2* promoter), intestine (*vha-6* promoter), chemosensory neurons (*odr-4* promoter) or acetylcholine (ACh) neurons (P*unc-17*) rescued the body morphology of *snf-3*, *egl-8* double mutants to normal (*egl-8* phenotype). Expression in the adult intestine (*vit-2* promoter) did not rescue the phenotypes. Error bars represent s.e.m. $^{***}P < 0.001$ compared with the *snf-3 egl-8* double mutant. The differences between the *egl-8* control and rescue of the *snf-3 egl-8* double mutant by expression of *snf-3*(+) in the excretory canal ($P = 0.0088$) or in the acetylcholine motor neurons ($P = 0.0031$) were statistically significant. Bottom, for the locomotion phenotype, the differences between *egl-8* control and rescue in the skin ($P = 0.0003$) and intestine ($P = 0.0048$) rescue were statistically significant. Expression of SNF-3 in the acetylcholine motor neurons did not rescue *snf-3 egl-8* locomotory defects ($P = 0.37$), possibly because SNF-3 activity is electrogenic and interferes with motor neuron function. ns indicates not statistically significant. Native tissues are cells that expressed the *snf-3* gene, whereas non-native tissues are cells in which *snf-3* gene expression was not detected. 11× outcrossed *snf-3*, *egl-8* is EG7513. Error bars represent s.e.m. The number of worms tested is shown inside each bar. (**c**) Tissue-specific rescue of the *egl-8* hypercontracted (top) and locomotion (bottom) phenotypes. *egl-8* cDNA was expressed in all cells (*dpy-30* promoter), neurons (*rab-3* promoter), acetylcholine neurons (*unc-17* promoter), intestine (*vha-6* promoter) or epidermis (*dpy-7* promoter). Expression of EGL-8 in acetylcholine neurons (*unc-17* promoter) generated transgenic worms that were long and loopy-coilers. The number of worms tested is shown inside each bar. Error bars represent s.e.m. $^{***}P < 0.001$. Statistical significance was determined using one-way ANOVA followed by Tukey *post hoc* comparisons. (**d**) Exogenous betaine slowed locomotion. (**e**) Overexpression of SNF-3 conferred resistance to excess betaine. The number of worms tested is shown inside each bar. Error bars represent s.e.m. Statistical significance was determined using one-way ANOVA followed by Tukey *post hoc* comparisons. $^{***}P < 0.001$, $^{**}P < 0.01$, ns (not significant) $P > 0.05$. (**f**) Average concentrations of total betaine in whole worms. These metabolites were identified using proton NMR spectroscopy. Statistical significance was determined using a one-way ANOVA on each metabolite with Bonferroni correction. $n = 8{,}000$ worms per strain. ns (not significant) $P > 0.05$, $^{*}P < 0.05$, $^{**}P < 0.01$, $^{***}P < 0.001$. Alleles are *egl-8(sa47)* and *snf-3(ox354)*, unless indicated otherwise.

concentration of betaine (250 mM) exhibited slowed swimming in the presence of betaine (**Fig. 3e**), whereas worms overexpressing the SNF-3 transporter were resistant to 250 mM betaine (**Fig. 3e**). These data suggest that excess betaine suppresses locomotion and that the SNF-3 betaine transporter clears betaine from the extracellular space.

snf-3 mutants exhibited locomotory phenotypes even if excess betaine was not applied (**Fig. 1c**,**d**), suggesting that betaine may already be present in worms. To determine betaine levels in *C. elegans*, we performed proton nuclear magnetic resonance (NMR) spectroscopic analysis on the worm metabolome. Betaine was present in extracts of worms at 7.0 ± 1.0 µM per mg of dry pellet (**Fig. 3f**), whereas the concentrations of GABA and acetylcholine were below detection (data not shown). Total betaine content did not change in *snf-3* mutants; however, a redistribution to the extracellular space would not be detectable in assays of whole worms. Notably, concentrations of the metabolites choline and glycine were higher in *snf-3* mutants (**Fig. 3f**). Levels of betaine in *C. elegans* are controlled in part by diet[29]. To confirm that our *E. coli* strains released betaine in the media, we measured the concentration of betaine in the media. We found that the bacterial media contained betaine at 2.3 ± 0.5 mM ml^{-1}, demonstrating that betaine was readily available from food.

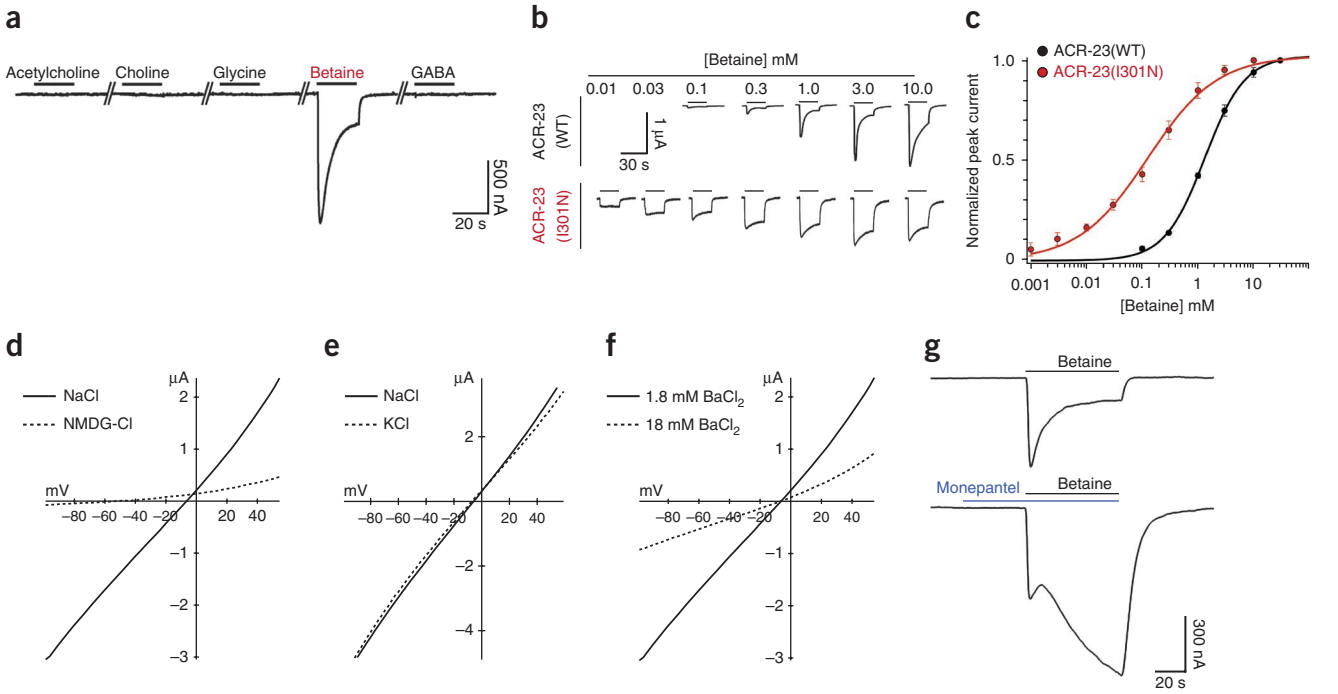

Figure 4 ACR-23 is a betaine-activated ion channel. (**a**) *Xenopus laevis* oocytes expressing ACR-23 responded to a 20-s pulse of 1 mM betaine, but not 1 mM acetylcholine, choline, glycine or GABA. The mean betaine-evoked response was 1.3 ± 0.13 µA for oocytes injected with 0.1 ng of cRNA (n = 9 oocytes). (**b**) Representative betaine-evoked currents from oocytes expressing wild-type ACR-23 (ACR-23(WT)) or ACR-23(I301N) stimulated with the indicated betaine concentration. (**c**) Betaine sensitivity of the wild-type ACR-23 channel (black line, n = 6 oocytes) and ACR-23(I301N) gain-of-function channel (red line, n = 5). EC_{50} was 1.4 mM for the wild type and 166 µM for ACR-23(I301N) (P = 0.0017). Error bars represent s.e.m. Statistical significance was determined using two-tailed unpaired Student's t test with Welch's correction. (**d**–**f**) ACR-23 is a monovalent cation channel. Insets indicate predicted ion flux under physiological conditions. (**d**) ACR-23 was permeable to sodium. Representative I-V curves in modified Ringer's solution containing Na^+ (n = 9) or NMDG (n = 8). (**e**) ACR-23 was potassium permeable. Representative I-V curves in modified Ringer's solution containing Na^+ (n = 7) or K^+ (n = 7). (**f**) ACR-23 was not permeable to the divalent cation Ba^{2+}. The reversal potential of betaine-evoked currents was not altered when the extracellular Ba^{2+} concentration was increased tenfold (n = 9). (**g**) Monepantel allosterically modulated ACR-23. A representative trace shows current induced by 1 mM betaine in the absence (above) or presence (below) of 300 pM monepantel in oocytes expressing ACR-23 (n = 11).

ACR-23 forms a homomeric betaine receptor

To test whether betaine acts directly on the ACR-23 receptor, we expressed ACR-23 in *Xenopus* oocytes and examined its response to various ligands. ACR-23 forms an ion channel that is activated by betaine, but not by acetylcholine, choline, glycine, or GABA (**Fig. 4a**). The sensitivity of ACR-23 for betaine is relatively weak; the half maximal concentration (EC_{50}) for betaine is 1.4 mM with a Hill coefficient of 1.2 ± 0.1 (**Fig. 4b**,**c**) compared to an EC_{50} of 40 µM for GABA receptors that function at the *C. elegans* neuromuscular junction[30]. Although we could not confirm the EC_{50} by recording from larval muscles *in vivo*, the sensitivity of the channel to betaine is consistent with the high K_m of the betaine transporter (~0.3 mM) and the concentrations of betaine found in extracellular space (~0.2 mM in mammals)[24].

ACR-23 is likely to be a nonselective monovalent cation channel. Similar to other cation channels, ACR-23 lacks a proline at the −2′ position and has a glutamate at the −1′ position of the TM2 pore-forming helix[31] (**Supplementary Fig. 2c**). Betaine-induced inward currents reversed at −9.4 ± 0.9 mV (**Fig. 4d**), which is consistent with a nonselective cation channel. To examine cation permeability, we replaced Na^+ in the extracellular solution with the large impermeant cation NMDG. NMDG largely abolished betaine-evoked inward currents and shifted the reversal potential to −42.8 ± 5.6 mV, indicating that monovalent cations contribute substantially to the ACR-23 current (**Fig. 4d**). To determine whether the ACR-23 channel is permeable to K^+ ions, we replaced external NaCl with KCl. These conditions did not cause a shift in the reversal potential (ΔE_{rev} = 0.6 ± 0.7 mV; **Fig. 4e**), indicating that the channel was also permeable to K^+ ions and exhibited no selectivity between Na^+ and K^+ (P_{Na}/P_K = 1.0). Two experiments revealed that ACR-23 exhibited little or no divalent cation permeability. First, we tested whether betaine-evoked currents could activate the endogenous Ca^{2+}-activated chloride channels in *Xenopus* oocytes, which can be activated by calcium, but not barium, influx through calcium-permeable ion channels[32]. However, replacement of extracellular Ca^{2+} with Ba^{2+} did not alter betaine-evoked currents in oocytes (data not shown). Second, increasing the concentration of Ba^{2+} tenfold failed to elicit a substantial shift in betaine-evoked reversal potential (ΔE_{rev} = 1.1 ± 1.1 mV; **Fig. 4f**). Thus, ACR-23 forms a homomeric betaine-gated ion channel that is nonselective for monovalent cations.

ACR-23 was first isolated as the target of the anthelmintic drugs known as AADs, commercially available as Zolvix, containing the AAD monepantel[14]. However, the pharmacological effects of this drug on the ACR-23 receptor have never been tested because the endogenous ligand of ACR-23 was not known[15]. To determine the effects of monepantel on ACR-23, we applied 300 pM monepantel (diluted Zolvix) to ACR-23–expressing oocytes. Monepantel did not elicit any current by itself, but instead potentiated betaine-induced currents (**Fig. 4g**). It was recently observed that 1,000-fold higher concentrations of monepantel (300 nM) can act as an agonist of ACR-23 (ref. 33). At 300 pM, monepantel did not activate the ion

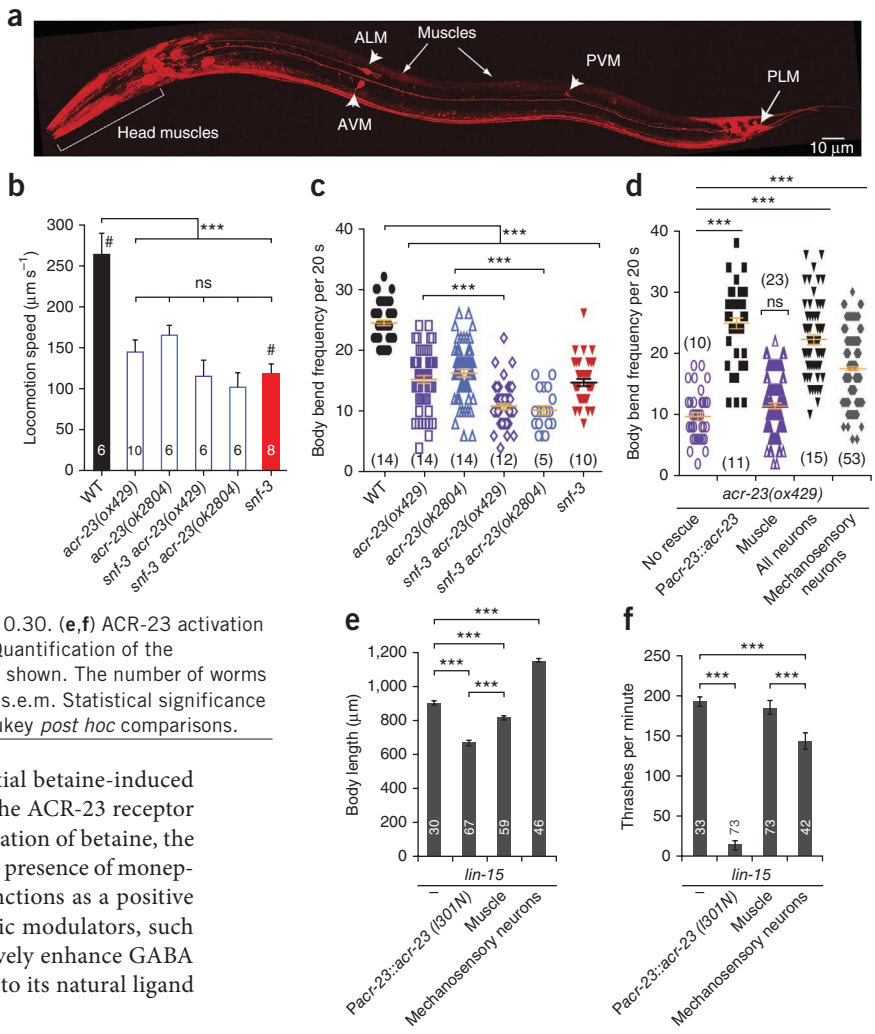

Figure 5 ACR-23 is required for sustained locomotion. (**a**) ACR-23 expression pattern. A transgenic hermaphrodite expressing mCherry driven by the *acr-23* promoter (P*acr-23*::*mCherry*::*let-858utr*) is shown. The strongest expression in the adult was in the mechanosensory neurons ALM, PLM, AVM and PVM (arrowheads), and head muscles (bracket). Expression was also seen in interneurons and body muscle. (**b**) Locomotion speed over a 5-min period on an agar plate without food. Speed was determined using an automated worm tracking system. # indicates data from **Figure 1d**. Data represent the mean ± s.e.m. ***$P < 0.001$, ns (not significant) $P > 0.05$. (**c**) Rate of body bends of worms on an agar plate. Each worm was tested four times in the absence of food. The number of worms tested is shown at the bottom of each column. Error bars represent s.e.m. (**d**) Neuronal expression rescued *acr-23* crawling defects. Error bars represent s.e.m. The number of worms tested is shown at the bottom of each column. Each worm was tested four times in the absence of food. ns indicates not significant relative to no rescue, $P = 0.30$. (**e**,**f**) ACR-23 activation reproduced *snf-3 egl-8* double mutant phenotypes. Quantification of the hypercontracted (**e**) and locomotion (**f**) phenotypes is shown. The number of worms tested is shown inside each bar. Error bars represent s.e.m. Statistical significance was determined using one-way ANOVA followed by Tukey *post hoc* comparisons.

channel and had no effect on the size of the initial betaine-induced current, but it did block the desensitization of the ACR-23 receptor (**Fig. 4g**). In addition, 60 s after the initial application of betaine, the current amplitude was 5.3 ± 0.9–fold larger in the presence of monepantel than in its absence. Thus, monepantel functions as a positive allosteric modulator of betaine gating. Allosteric modulators, such as benzodiazepines and barbiturates that positively enhance GABA transmission, alter the response of the receptor to its natural ligand without competing for the binding site.

ACR-23 acts in the nervous system to regulate locomotion

To determine where ACR-23 functions during locomotion, we characterized the expression pattern of the *acr-23* gene using transcriptional mCherry reporter constructs (**Fig. 5a** and **Supplementary Fig. 2b**). *acr-23* was expressed strongly in the six mechanosensory neurons, multiple interneurons and body muscles. ACR-23 expression in muscle was high in larvae and weak in adults. The expression of *acr-23* in the larval body muscles was consistent with the hypercontraction phenotype observed in *snf-3 egl-8* double mutants.

The lack of expression in motor neurons was surprising to us because mutants lacking *acr-23* (**Supplementary Fig. 1c**) exhibited mild swimming defects (**Fig. 1g**), were lethargic when crawling on an agar plate (**Fig. 5b**,**c**) and their movement was interrupted by frequent pauses. *snf-3* mutants and *snf-3 acr-23* double mutants were equally sluggish (**Figs. 1g** and **5b**,**c**), suggesting that the effect of betaine on locomotion is mediated by different receptors.

To determine where ACR-23 functions during locomotion, we rescued the mutant using tissue-specific promoters. Expression in the nervous system rescued the locomotory phenotypes of *acr-23* mutants (**Fig. 5d**). Expression in the mechanosensory neurons also partially restored motor activity (**Fig. 5d**), consistent with the known role of these cells in controlling basal levels of locomotion[34]. Thus, as with *egl-8*, *acr-23* is required in the nervous system. These data suggest that phospholipase Cβ limits ACR-23 function in the nervous system, either directly or indirectly.

Gain-of-function ACR-23 resembles *snf-3 egl-8* mutant

Together, these data suggest that an increase in betaine levels in the *snf-3 egl-8* double mutants inappropriately activates ACR-23 and leads to hypercontraction. To demonstrate that constitutive activation of ACR-23 could generate the hypercontracted phenotype, we generated an ACR-23 receptor with a higher ligand sensitivity. The second transmembrane domain forms the pore in ligand-gated ion channels and the residues are numbered 0′ to 19′ by convention[35]. Mutations at the 13′ position of the pore are known to increase the ligand sensitivity and conductance of cys-loop ion channels, probably by affecting transitions to the open state[31]. We engineered a variant at the 13′ position, ACR-23(I301N), based on known gain-of-function mutations in a related receptor[36] (**Supplementary Fig. 2c**). Similar to other receptors[31], ACR-23(I301N) was more sensitive to betaine and the channel desensitized less than the wild-type receptor (**Fig. 4c**). The EC_{50} for the receptor decreased eightfold, from 1,400 µM to 166 µM (**Fig. 4c**).

This hypersensitive variant of ACR-23 in transgenic worms recapitulated the *snf-3 egl-8* double mutant phenotype. Most ACR-23(I301N) transgenic worms died during larval development. Those that escaped lethality and reached adulthood were severely hypercontracted (**Supplementary Fig. 2d** and **Fig. 5e**) and uncoordinated (**Fig. 5f**), closely resembling the phenotype of *snf-3 egl-8* mutants. We also evaluated the tissue-specific effects of the gain-of-function ACR-23(I301N) mutation. Expressing ACR-23(I301N) in body

muscles alone generated hypercontracted worms that only exhibited modest locomotion defects (**Fig. 5e**,**f** and **Supplementary Fig. 2e**). Conversely, expression of ACR-23(I301N) in the mechanosensory neurons resulted in morphologically wild-type worms that exhibited uncoordinated thrashing in liquid (**Fig. 5e**,**f** and **Supplementary Fig. 2d**). These data are consistent with ACR-23 acting in part via the nematode somatosensory circuit to modulate locomotion.

DISCUSSION

Using two forward genetic screens, we uncovered the molecular pathway that leads to betaine toxicity in nematodes. ACR-23 is a betaine-gated cation channel expressed in body muscle and neurons. The betaine transporter SNF-3 removed betaine from the extracellular space (**Supplementary Fig. 4**). In the absence of *snf-3*, betaine was able to accumulate in the extracellular space, and *snf-3* mutants exhibited subtle locomotory phenotypes. These phenotypes were exacerbated by mutations in phospholipase Cβ. In the *snf-3 egl-8* double mutant, constitutive activation of ACR-23 led to hypercontraction, paralysis and sometimes death as a result of a combination of effects on the nervous system and muscle. Why phospholipase Cβ mutations are synthetic with mutations in the transporter is not clear; however, one possibility is that phospholipase Cβ is required to downregulate ACR-23 itself or the activity of the neurons in which it functions. Thus, the elimination of the receptor by mutation restores muscle function and locomotion, reversing the effect of the *snf-3* and *egl-8* mutations.

In addition to its natural ligand betaine, ACR-23 is also the target of a class of anthelmintic drugs known as AADs, which contain the active compound monepantel[14]. Monepantel induces muscle hypercontraction, spasmodic pharyngeal contraction, paralysis and death in *C. elegans*[14]. These characteristics are shared with other anthelmintic drugs that activate ligand-gated ion channels in the nematode. Unlike these receptor agonists, monepantel acted as an allosteric modulator of ACR-23, potentiating betaine signaling during development, resulting in nematode death. A drawback of monepantel is that some of the genera lacking the *acr-23* gene include parasitic nematodes[23], such as *Strongyloides* and *Ascaris*, which represent a major public health concern in developing countries. Unlike *acr-23*, SNF-3 has an ortholog in most parasitic nematodes species with a sequenced genome. Thus, the betaine–SNF-3 pathway offers a unique set of targets that can be used to improve AAD efficiency or to develop new anthelmintic drugs.

What then is the normal role of betaine in the nematode? Betaine signaling was required in *C. elegans* for basal levels of locomotion: *acr-23* mutants were sluggish when crawling on agar. The effect on locomotion was mediated in part via ACR-23 receptors expressed in the mechanosensory neurons. The mechanosensory neurons innervate the locomotory command neurons to stimulate touch-induced movement as well as spontaneous levels of locomotion[37,38]. The mechanosensory neuron dendritic processes run adjacent to the epidermis and, in some cases, are completely embedded in the epidermal cells expressing the betaine clearance transporter SNF-3. We cannot exclude the possibility that betaine is acting as a conventional neurotransmitter, that is, that it is released onto neurons and muscles at synapses. However, it is also possible that betaine is released by the epidermis rather than by neurons. In this model, the skin may both release betaine onto the mechanosensory processes and clear it from the space between the skin and dendrite, acting as both source and sink for this neurotransmitter.

Betaine has been shown to have anticonvulsant properties in vertebrate brain[5–7], but its mechanisms of action have not been elucidated. Although *acr-23* is not conserved in the vertebrate, *snf-3* and phospholipase Cβ are conserved and expressed in the vertebrate nervous system. The mammalian nervous system contains many uncharacterized ligand-gated ion channels and G protein–coupled receptors. Some of these could potentially mediate betaine anticonvulsive properties.

METHODS

Methods and any associated references are available in the online version of the paper.

Note: Any Supplementary Information and Source Data files are available in the online version of the paper.

ACKNOWLEDGMENTS

We thank E.M. Peden (University of Utah) for comments and input on the manuscript, J. Rand and G. Mullen (Oklahoma Medical Research Foundation) and the *Caenorhabditis* Genetics Center for providing strains, M.W. Davis and C. Thacker (University of Utah) for Illumina sequencing analysis, A. Fire (Stanford University) for providing the GFP expression vectors, Z.W. Wang (University of Connecticut) for the worm tracker, and H.-F. Han, J.W. Gardner and D. Maxfield (University of Utah) for help with locomotion assays. We also thank R. Gasser (University of Melbourne) for his generous gift of Zolvix. This work was supported by grants from the US National Institutes of Health (AG22468 to Y.-J.F., NS034307 to E.M.J. and National Research Service Award F32GM084596 to A.S.P.) and the National Science Foundation (IOS-0920069 to E.M.J.). E.M.J. receives funding from the Howard Hughes Medical Institute.

AUTHOR CONTRIBUTIONS

A.S.P. designed and performed genetics screens and behavior analyses, and wrote the paper. Y.-J.F., G.J. and V.G. designed and performed the physiological analyses of the betaine transporter. P.M. performed the physiological analyses of the betaine receptor. J.L.G. and C.C. measured betaine concentrations in the worm using NMR spectroscopy. E.A.M. and K.J.M. helped J.L.G. with nematode cultures. E.M.J. provided guidance and edited the paper.

COMPETING FINANCIAL INTERESTS

The authors declare no competing financial interests.

1. Morgan, K. & Tarjan, A. Management of sting nematode on centipede grass with kelp extracts. *Proc. Fla. State Hort. Soc.* **93**, 97–99 (1980).
2. Wu, Y., Jenkins, T., Blunden, G., Whapham, C.A. & Hankins, S.D. The role of betaines in alkaline extracts of Ascophyllum nodosum in the reduction of *Meloidogyne javanica* and *M. incognita* infestations of tomato plants. *Fundam. Appl. Nematol.* **20**, 99–102 (1997).
3. Whapham, C.A., Jenkins, T., Blunden, G. & Hankins, S.D. The role of seaweed extracts, *Ascophyllum nodosum*, in the reduction in fecundity of Meloidogyne javanica. *Fundam. Appl. Nematol.* **17**, 181–183 (1994).
4. Wu, Y., Jenkins, T., Blunden, G., von Mende, N. & Hankins, S. Suppression of fecundity of the root-knot nematode, *Meloidogyne javanica*, in monoxenic cultures of *Arabidopsis* thaliana treated with an alkaline extract of Ascophyllum nodosum. *J. Appl. Phycol.* **10**, 91–94 (1998).
5. Ghoz, E.H. & Freed, W.J. Effects of betaine on seizures in the rat. *Pharmacol. Biochem. Behav.* **22**, 635–640 (1985).
6. Freed, W.J., Gillin, J.C. & Wyatt, R.J. Anticonvulsant properties of betaine. *Epilepsia* **20**, 209–213 (1979).
7. Wuerthele, S.E., Yasuda, R.P., Freed, W.J. & Hoffer, B.J. The effect of local application of homocysteine on neuronal activity in the central nervous system of the rat. *Life Sci.* **31**, 2683–2691 (1982).
8. Zhu, X.-M. & Ong, W.-Y. A light and electron microscopic study of betaine/GABA transporter distribution in the monkey cerebral neocortex and hippocampus. *J. Neurocytol.* **33**, 233–240 (2004).
9. Lewis, J.A., Wu, C.H., Berg, H. & Levine, J.H. The genetics of levamisole resistance in the nematode *Caenorhabditis elegans*. *Genetics* **95**, 905–928 (1980).
10. Lewis, J.A., Wu, C.H., Levine, J.H. & Berg, H. Levamisole-resistant mutants of the nematode *Caenorhabditis elegans* appear to lack pharmacological acetylcholine receptors. *Neuroscience* **5**, 967–989 (1980).
11. Dent, J.A., Davis, M.W. & Avery, L. avr-15 encodes a chloride channel subunit that mediates inhibitory glutamatergic neurotransmission and ivermectin sensitivity in *Caenorhabditis elegans*. *EMBO J.* **16**, 5867–5879 (1997).
12. Arena, J.P., Liu, K.K., Paress, P.S., Schaeffer, J.M. & Cully, D.F. Expression of a glutamate-activated chloride current in *Xenopus* oocytes injected with *Caenorhabditis elegans* RNA: evidence for modulation by avermectin. *Brain Res. Mol. Brain Res.* **15**, 339–348 (1992).

13. Cully, D.F. *et al.* Cloning of an avermectin-sensitive glutamate-gated chloride channel from *Caenorhabditis elegans*. *Nature* **371**, 707–711 (1994).
14. Kaminsky, R. *et al.* A new class of anthelmintics effective against drug-resistant nematodes. *Nature* **452**, 176–180 (2008).
15. Rufener, L., Baur, R., Kaminsky, R., Maser, P. & Sigel, E. Monepantel allosterically activates DEG-3/DES-2 channels of the gastrointestinal nematode Haemonchus contortus. *Mol. Pharmacol.* **78**, 895–902 (2010).
16. Lackner, M.R., Nurrish, S.J. & Kaplan, J.M. Facilitation of synaptic transmission by EGL-30 Gqalpha and EGL-8 PLCbeta: DAG binding to UNC-13 is required to stimulate acetylcholine release. *Neuron* **24**, 335–346 (1999).
17. Miller, K.G., Emerson, M.D. & Rand, J.B. Goalpha and diacylglycerol kinase negatively regulate the Gqalpha pathway in *C. elegans*. *Neuron* **24**, 323–333 (1999).
18. Torres, G.E., Gainetdinov, R.R. & Caron, M.G. Plasma membrane monoamine transporters: structure, regulation and function. *Nat. Rev. Neurosci.* **4**, 13–25 (2003).
19. Hahn, M.K. & Blakely, R.D. The functional impact of SLC6 transporter genetic variation. *Annu. Rev. Pharmacol. Toxicol.* **47**, 401–441 (2007).
20. Giros, B., Jaber, M., Jones, S.R., Wightman, R.M. & Caron, M.G. Hyperlocomotion and indifference to cocaine and amphetamine in mice lacking the dopamine transporter. *Nature* **379**, 606–612 (1996).
21. Sawin, E.R., Ranganathan, R. & Horvitz, H.R. *C. elegans* locomotory rate is modulated by the environment through a dopaminergic pathway and by experience through a serotonergic pathway. *Neuron* **26**, 619–631 (2000).
22. McDonald, P.W. *et al.* Vigorous motor activity in *Caenorhabditis elegans* requires efficient clearance of dopamine mediated by synaptic localization of the dopamine transporter DAT-1. *J. Neurosci.* **27**, 14216–14227 (2007).
23. Rufener, L., Keiser, J., Kaminsky, R., Mäser, P. & Nilsson, D. Phylogenomics of ligand-gated ion channels predicts monepantel effect. *PLoS Pathog.* **6**, e1001091 (2010).
24. Yamauchi, A. *et al.* Cloning of a Na^+- and Cl-dependent betaine transporter that is regulated by hypertonicity. *J. Biol. Chem.* **267**, 649–652 (1992).
25. Borden, L.A., Smith, K.E., Gustafson, E.L., Branchek, T.A. & Weinshank, R.L. Cloning and expression of a betaine/GABA transporter from human brain. *J. Neurochem.* **64**, 977–984 (1995).
26. Hoffmann, E.K., Lambert, I.H. & Pedersen, S.F. Physiology of cell volume regulation in vertebrates. *Physiol. Rev.* **89**, 193–277 (2009).
27. Craig, S.A. Betaine in human nutrition. *Am. J. Clin. Nutr.* **80**, 539–549 (2004).
28. Mullen, G.P. *et al.* The *Caenorhabditis elegans* snf-11 gene encodes a sodium-dependent GABA transporter required for clearance of synaptic GABA. *Mol. Biol. Cell* **17**, 3021–3030 (2006).
29. Reinke, S.N., Hu, X., Sykes, B.D. & Lemire, B.D. *Caenorhabditis elegans* diet significantly affects metabolic profile, mitochondrial DNA levels, lifespan and brood size. *Mol. Genet. Metab.* **100**, 274–282 (2010).
30. Bamber, B.A., Beg, A.A., Twyman, R.E. & Jorgensen, E.M. The *Caenorhabditis elegans* unc-49 locus encodes multiple subunits of a heteromultimeric GABA receptor. *J. Neurosci.* **19**, 5348–5359 (1999).
31. Galzi, J.-L. *et al.* Mutations in the channel domain of a neuronal nicotinic receptor convert ion selectivity from cationic to anionic. *Nature* **359**, 500–505 (1992).
32. Vernino, S., Amador, M., Luetje, C.W., Patrick, J. & Dani, J.A. Calcium modulation and high calcium permeability of neuronal nicotinic acetylcholine receptors. *Neuron* **8**, 127–134 (1992).
33. Rufener, L. *et al.* acr-23 Encodes a monepantel-sensitive channel in *Caenorhabditis elegans*. *PLoS Pathog.* **9**, e1003524 (2013).
34. Chalfie, M. & Sulston, J. Developmental genetics of the mechanosensory neurons of *Caenorhabditis elegans*. *Dev. Biol.* **82**, 358–370 (1981).
35. Keramidas, A., Moorhouse, A.J., Schofield, P.R. & Barry, P.H. Ligand-gated ion channels: mechanisms underlying ion selectivity. *Prog. Biophys. Mol. Biol.* **86**, 161–204 (2004).
36. Treinin, M. & Chalfie, M. A mutated acetylcholine receptor subunit causes neuronal degeneration in *C. elegans*. *Neuron* **14**, 871–877 (1995).
37. Driscoll, M. & Kaplan, J. Mechanosensory control of locomotion. in *C. elegans II*, 2nd edn. (eds. Riddle, D.L., Blumenthal, T., Meyer, B.J. & Priess, J.R.) Ch. 23 (Cold Spring Harbor Laboratory Press, 1997).
38. Chalfie, M. *et al.* The neural circuit for touch sensitivity in *Caenorhabditis elegans*. *J. Neurosci.* **5**, 956–964 (1985).

ONLINE METHODS

Enhancer screen. We mutagenized EG4094 *egl-8(sa47) V; oxEx771[B0348 egl-8(+); rol-6(sd);* P*myo-2::GFP]* with 20 nM ENU. B0348 is a cosmid that rescues *egl-8*. We singled individual F_1 and F_2 offspring carrying the *plcβ* rescuing extrachromosomal array *oxEx771[B0348 (egl-8*$^{+}$*; rol-6(sd);* P*myo-2::GFP]*. We screened F_3 offspring for the presence of an enhancer by looking for new phenotypes in non-GFP–expressing siblings (*plcβ* mutant background) that were not observed in GFP-expressing siblings (*plcβ* rescued). We screened 1,669 haploid genomes and isolated *snf-3(ox354)* from this screen.

We mapped *snf-3(ox354)* to the left arm of chromosome II using single nucleotide polymorphism mapping[39]. The region was further narrowed by rescuing *snf-3* using standard microinjection transgenic techniques[40]. *snf-3(ox354)* was rescued by injecting *snf-3(ox354)*, *egl-8(sa47)* worms with a pool of cosmids F45D11, M01D1 and C07D2 along with 2 ng μl^{-1} P*myo-2::GFP* co-injection marker. Each cosmid was injected at 20 ng μl^{-1}. Cosmid C07D2 alone was sufficient to rescue the *snf-3(ox354)* enhancer defects. We were able to rescue *snf-3(ox354)* by injecting four overlapping PCR fragments from wild-type genomic DNA of the T13B5.1 gene. To identify the molecular lesion in *snf-3(ox354)*, we sequenced *snf-3* PCR fragments generated from *snf-3(ox354) egl-8(sa47)* double mutant worms.

Suppressor screen. We mutagenized EG7081 *snf-3(ox354) egl-8(sa47)* with 20 nM ENU. We screened the F_2 progeny for non-hypercontracted and non-uncoordinated worms. We screened a total of 37,000 haploid genomes. We isolated *acr-23(ox429)* from this screen.

To identify the mutation *ox429,* we resequenced the genome of EG6501 *snf-3(ox354) egl-8(sa47) acr-23(ox429)* using an Illumina Genome Analyzer II (GAII). The molecular lesion in *acr-23(ox429)* was confirmed using traditional Sanger sequencing. To rescue *acr-23(ox429),* we injected *snf-3 egl-8 acr-23* triple mutants (EG6501) with either four overlapping PCR fragments with a 1-kb overlap (25 ng μl^{-1} each) of *acr-23* genomic DNA or a full-length *acr-23* gene with 2 ng μl^{-1} P*myo-2::mCherry* co-injection marker. From injections of these two constructs, we obtained over ten transgenic lines with the restoration of the hypercontracted phenotype observed in simple *snf-3 egl-8* double mutants. Most of these transgenic strains were very sick and hard to maintain. We further confirmed that *ox429* was an allele of *acr-23* by crossing a null allele of *acr-23(ok2804)* into *snf-3 egl-8* double mutants to generate *snf-3 egl-8 acr-23(ok2804)* (EG6544) worms.

Molecular biology. To create a full-length genomic *snf-3* DNA plasmid, we excised a 15-kb genomic fragment of *snf-3* from C07D2 using StuI and restriction digest and ligated it into pLITMUS38 (pADA49). To generate a fluorescently tagged SNF-3, we cut the GFP with MluI from the pPD114.24 vector (A. Fire, Stanford University), and ligated it into an MluI site in the largest intron in frame with the gene to generate pADA65. The GFP tag is located in the extracellular loop between transmembrane domain 9 and 10. 30 ng μl^{-1} of pADA65 was injected in *snf-3(ox354) egl-8(sa47)* along with 2 ng μl^{-1} P*myo-3::mCherry* and P*unc-122::GFP* co-injection marker. Multiple transgenic lines were obtained and they fully rescued *snf-3(ox354)* enhancer defects (strain EG4769 carries *oxEx1067*). We also tagged SNF-3 at the N terminus by ligating P*snf-3* and the *snf-3* coding region into the GFP vector pPD117.01 (A. Fire) to generate pADA73. 10 ng μl^{-1} of pADA73 was injected into *lin-15(n765ts)* along with 2 ng μl^{-1} P*myo-3::mCherry* co-injection marker and *lin-15(+)*(pL15EK). We generated EG6888 from these injections. To visualize neurons expressing SNF-3::GFP, we subjected EG6888 to RNAi feeding plates against GFP (pPD128.110). For tissue-specific rescue, we used the MultiSite Gateway Pro 3-fragment recombination technology (Invitrogen, catalog no.12537-023). All constructs containing a promoter were inserted into the pDONR P4-P1 vector (slot 1). These promoters contained the initiating start codon (ATG). *snf-3* cDNA, lacking the ATG, was inserted into the pDONR 221 vector (slot 2). The C-terminal tag fluorescent protein (GFP or mCherry) followed by the 3′UTRs of *unc-54* or *let-858* gene were inserted into pDONR P2R-P3 vector (slot 3). The final recombination product was inserted into pDEST R4-R3 vector.

To create rescuing constructs for *egl-8,* we used MultiSite Gateway Technology. *egl-8* cDNA without an ATG was inserted into the pDONR 221 vector (slot 2).

To create a full-length genomic *acr-23* construct, we divided the genomic region into three fragments that were inserted into different Multisite Gateway pDONR vectors. A 2.9-kb promoter and the full genomic region except for the last two exons of the gene were inserted into the pDONR P4-P1 vector. The 4-kb intron and exon 8 were inserted into the pDONR 221 vector, and the last exon and the 3′ UTR (252 bases) were inserted into pDONR P2R-P3 vector. These three fragments were recombined with pDEST R4-R3 vector to create pADA246. To create pASP268, we inserted mCherry in operon between the last exon of the gene and the 3′ UTR in the pDONR P2R-P3 vector using Gibson Assembly Cloning technology (New England Biolab). The intergenic region of the *gdp-2 gdp-3* was used to express mCherry from an operon. All the constructs used for tissue specific rescues were created using the MultiSite Gateway Technology. An *acr-23* cDNA containing an ATG was inserted into the pDONR 221 vector. In this case, the corresponding promoters (P*myo-3*, P*rab-3* and P*mec-7*) in slot 1 lack ATG.

Confocal microscopy. We acquired images of fluorescently tagged fusion proteins in living *C. elegans* with a 63× 1.4 NA oil objective on a Pascal LSM5 confocal microscope (Carl Zeiss).

Body length assay. We selected L4 worms the day before the assay for each genotype studied. On the day of the experiment, we anesthetized adult worms with 15 mM sodium azide in M9 solution on freshly made 2% agarose pads. We used a plan-Neofluar 10× 0.3 NA objective on a Pascal LSM5 confocal microscope. The size of the worm was determined using a build-in function on the LSM5 image browser.

Growth assay. We plated 10 L4 larvae on NGM plates 12 h before we started the experiment. We transferred the adults every 6.5 h (at 22.5 °C) or overnight (12 h) at 15 °C. After the animals were transferred, we counted the number of eggs laid. We monitored hatching rate and development rate to adulthood. Adulthood was determined by the presence of a vulva. The percentage of worms was normalized to each plate.

Betaine assay. We top-spreaded NGM plates with betaine to obtain a final concentration of 50 and 250 mM. These plates were allowed to dry at 22.5 °C for 24 h and then seeded with the *E. coli* strain OP50. On the day of the experiment, we added three L4 worms to each plate. The plates were coded so the experimenter was blind to betaine concentrations and genotype of the strains. The first and second generations progeny were then tested in a thrashing assay. For the *snf-3* overexpression line (EG8093), the array *oxEx1208* was crossed out from strain EG5051 and crossed twice against N2.

Thrashing assay for locomotion. Single young adult worms were placed in a microtiter well in a 96-well plate without agar, containing 150 µl of water. Assays in M9 yielded similar results (data not shown). The worm was allowed to acclimate for 2 min and we counted thrashes for 60 s. One thrash reflects the bending of the body from the midbody toward one side of the animal and back again. The value obtained is doubled to reflect the true number of bends.

Crawling assay for locomotion. We transferred well-fed young adult worms to a food-free NGM plate (100 mm). Worms were allowed to acclimate for 5 min and we counted the number of body bends generated by each worm every 20 s. Each worm was tested four times.

Crawling speed assay. The speed of the worm was determined using an automated worm tracking and analysis system. A single young adult worm was transferred to a food-free NGM plate (100 mm) placed on a motorized microscope stage (OptiScan ES111, Prior Scientific). After a 1-min acclimation period, the worm was imaged at 5 frames per s for 5 min using a VGA FireWire camera (XCD-V60, Sony) mounted on a Leica MS5 stereomicroscope. A custom MATLAB program[41] (MathWorks) was used to control the camera and the motorized stage and to determine the mean locomotion speed. The speed was calculated based on the distance traveled by the worm over 5 min.

Statistical analysis. Statistical analyses were performed using Kaleidagraph 3.6 and GraphPad Prism 6. All grouped data are reported as means ± s.e.m.

doi:10.1038/nn.3575

Statistical significance between genotypes was determined using one-way ANOVA followed by Tukey *post hoc* comparisons. We used two-tailed unpaired Student's *t* test with Welch's correction to determine the difference between wild-type and the gain-of-function (**Fig. 4c**). Logarithmic normal distribution was assumed for betaine EC_{50} values, so we use the pEC_{50} values for statistical analysis. $P < 0.05$ was considered statistically significant. No statistical methods were used to predetermine sample sizes, but our sample sizes are similar to those reported in previous publications in the field (thrash assay[42], speed[41], body bends[21] and body length[43]). Data distributions were assumed to be normal, but this was not formally tested. Data collection and analysis were not always performed blind, but we specifically state which experiments were performed blind in the Online Methods. All of the data were collected and processed side by side in a randomized manner.

SNF-3 transport assay in HRPE cells. HRPE cells were transfected using a vaccinia virus expressing *snf-3* cDNA as described previously[44,45]. HRPE cells grown in 24-well plates were infected with a recombinant vaccinia virus (VTF7-3). This virus carries the gene for T7 RNA polymerase. The virus was allowed to adsorb onto the cells for 30 min at 37 °C with gentle shaking of the plate. Cells were then transfected with the plasmid DNA (empty vector pSPORT1 or *snf-3* cDNA construct) using the lipofection procedure (Invitrogen). The cells were incubated at 37 °C for 12 h and then assayed for transport activity. The uptake of [^{14}C]betaine (2.5 μM) was determined at 37 °C. In most experiments, the media consisted of 25 mM Hepes/Tris (pH 7.5), 140 mM NaCl, 5.4 mM KCl, 1.8 mM $CaCl_2$, 0.8 mM $MgSO_4$, and 5 mM glucose. In experiments in which the cation and anion dependence of the transport process was investigated, NaCl was replaced isoosmotically by sodium gluconate or NMDG chloride. Uptake measurements were routinely made in parallel in control cells transfected with vector alone and in cells transfected with the vector-cDNA construct. The uptake activity in cDNA-transfected cells was adjusted for the endogenous activity measured in control cells to calculate the cDNA-specific activity. Experiments were performed in triplicate, and each experiment was repeated at least three times. Results are presented as means ± s.e.m. The kinetic parameters, Michaelis-Menten constant (K_m) and maximal velocity (V_{max}) were calculated by fitting the data to a Michaelis-Menten equation describing a single saturable transport system. Analysis was done by nonlinear regression, and the resultant values for the kinetic parameters were confirmed by linear regression.

SNF-3 analysis. The procedures for cRNA *in vitro* transcription, *Xenopus laevis* oocyte isolation, microinjection, superfusion, voltage clamping and data analysis have been described previously[45,46]. Briefly, the plasmid SNF-3 :: pSPORT1 was linearized with NotI and transcribed *in vitro* to cRNA using the mMESSAGE mMACHINE RNA transcription kit (Ambion). The expression of SNF-3 was initially detected by comparing the uptake of (2.5 μM) [^{14}C]-betaine (55 mCi mmol^{-1}, American Radiolabeled Chemicals) in water-injected oocytes versus SNF-3–injected oocytes. The electrophysiological characteristics of the heterologously expressed SNF-3 were then studied using a GeneClamp 500 (Axon Instruments). Kinetic parameters for the saturable transport of SNF-3 were calculated using the Michaelis-Menten equation. Data were analyzed by nonlinear regression and confirmed by linear regression.

ACR-23 analysis. ACR-23 analysis was performed as described previously[47]. To generate plasmid constructs for *Xenopus* oocyte expression, we subcloned full-length error-free ACR-23 cDNAs and ACR-23 gain-of-function (ACR-23(I301N)) into the pSGEM expression vector using the SLIC cloning technique[48] to produce pADA206 and pADA278. RNAs were prepared using the T7 mMessage mMachine kit (Ambion). Capped ACR-23 (0.1–5 ng total) or ACR-23(I301N) (0.5–2.5 ng total) RNAs were injected into *Xenopus* oocytes. 1–4 d post-injection, two-electrode voltage-clamp recordings were performed. Voltage was clamped at −60 mV. The standard bath solution was Ringer's: 115 mM NaCl, 2.5 mM KCl, 1.8 mM $CaCl_2$, 10 mM Hepes, pH 7.2 (NaOH). Each oocyte was subjected to 20-s applications of agonist with a 2-min wash between test applications. Expression of ACR-23(I301N) was very toxic to *Xenopus* oocytes. We only used healthy oocytes with low channel expression for further analysis of this receptor. Eight oocytes were used to characterize the betaine concentration-response relationship of ACR-23(I301N), but individual oocytes were not tested through the full range of active concentrations. Three oocytes were tested at 0.001–0.003 mM, five were tested at 0.01–0.3 mM, and all were tested at 1–10 mM. Curves were fit to data from the five oocytes with data in the linear response range to perform statistical analysis of EC_{50} values.

Ion selectivity. For voltage-ramp experiments, $CaCl_2$ was replaced by $BaCl_2$ in the extracellular solutions to eliminate possible contributions from the endogenous Ca^{2+}-activated chloride channel. To assay sodium permeability, we substituted 115 mM NMDG chloride for NaCl. Thus, Na-free solution contains 115 mM NMDG, 2.5 mM KCl, 1.8 mM $BaCl_2$, and 10 mM Hepes, pH 7.2 (HCl). To compare sodium and potassium permeability, NaCl was replaced with equimolar KCl: 115 mM KCl, 2.5 mM NaCl, 1.8 mM $BaCl_2$, 10 mM Hepes, pH 7.2 (KOH). To assay barium permeability, $BaCl_2$ was increased tenfold: 115 mM NaCl, 18 mM $BaCl_2$, 2.5 mM KCl, 10 mM HEPES, pH 7.2 (NaOH). The osmolarity of each solution was adjusted to 300 mOsm with sucrose. Reversal potentials were measured using 2-s voltage ramps (−100 mV to +60 mV) during sustained betaine application. Reversal potential shifts were similar at various time points after initiating betaine perfusion. Ramps at 20 s were analyzed for the potassium substitution experiment because of changing rectification characteristics at later time points, whereas ramps at 60 s were used for all other analyses. An agar bridge was used to minimize changes in junction potentials when switching solutions. Small residual voltage offsets due to differing ion composition in perfusion buffers were measured relative to standard solution before each voltage ramp recording, and were subtracted from the amplifier command voltages during data analysis. Data analysis was performed using Igor software (WaveMetrix). All chemicals were purchased from Sigma Chemical.

Monepantel. Commercially available Zolvix (25 mg ml^{-1} monepantel, Novartis) was diluted in DMSO to make a 10 mM stock solution of monepantel. The stock solution was diluted in water to make a 10 μM working stock in 0.1% DMSO. Final concentrations were achieved by diluting in Ringer's to make the experimental perfusion solutions. 1 mM betaine was applied for 60 s either alone or in the presence of 0.3 nM monepantel following a 40-s pre-application of monepantel alone. All perfusion buffers were supplemented with 0.1% DMSO. Peak current magnitudes in three 10-s time windows were compared in the presence and absence of monepantel immediately after applying monepantel alone, immediately after initiating betaine application and 50 s after sustained betaine application.

Culture of nematodes. Strain genotypes were blinded to the experimenter. Early embryos were isolated by alkaline hypochlorite treatment and plated after synchronization on NGM plates seeded with HB101 bacteria as a food source at 20 °C. For each biological replicate, ~8,000 worms were harvested, washed twice with M9, twice with water and stored at −80 °C until extraction. Eight samples were grown for each strain.

Extraction procedure for metabolites. Metabolites from whole nematodes were extracted using a methanol-chloroform procedure. 600 μl of a methanol-chloroform mix (2:1, vol/vol) was added to the frozen nematodes. Samples were homogenized using a Polytron and sonicated for 15 min. 200 μl each of chloroform and water were added, the samples centrifuged and the aqueous layer separated from the lipid one. The procedure was repeated twice. The aqueous layer was dried overnight in an evacuated centrifuge.

Analysis of aqueous extracts. The dried extracts were rehydrated in 600 μl of D_2O containing 0.05 mM sodium-3-(tri-methylsilyl)-2,2,3,3-tetradeuteriopropionate (TSP; Cambridge Isotope Laboratories) as an internal standard. The samples were analyzed using an AVANCE II+ NMR spectrometer operating at 500.13 MHz for the ^{1}H frequency (Bruker) using a 5-mm TXI probe. Spectra were collected using a solvent suppression pulse sequence based on a one-dimensional NOESY pulse sequence to saturate the residual ^{1}H water signal (relaxation delay = 2 s, t_1 increment = 3 μs, mixing time = 150 ms, solvent presaturation applied during the relaxation time and the mixing time). 196 transients were collected into 16 K data points over a spectral width of 12 ppm at 27 °C for the adult samples.

Analysis of the metabolic profile of the bacteria. 400 µl of the bacteria (HB101) broth used to feed worms was mixed with 600 µl of water and centrifuged. The supernatant was collected and dried in an evacuated centrifuge. The dried samples were rehydrated in 600 µl D_2O, containing 0.05 mM TSP as an internal standard and analyzed by NMR spectroscopy in the same way as the extracts described above. 128 transients were collected for these samples.

Data processing. NMR spectra were processed using an ACD one-dimensional NMR processor (version 13, ACD). Free induction decays were Fourier transformed following multiplication by a line broadening of 1 Hz, and referenced to TSP at 0.0 ppm. Spectra were phased and baseline corrected manually. Each spectrum was integrated using 0.02 ppm integral regions between 0.5 and 4.5, and 5.5–9.5 ppm. Each spectral region was normalized to a total integral value of 1,000. In addition the resonances of selected metabolites (betaine, choline and glycine) were integrated using the software package Chenomx version 7.1. The integrals were normalized to total pellet dry weight.

Multivariate analysis of metabolic profiles. Each set of metabolic profiles obtained were analyzed by multivariate analysis. Data sets were imported into SIMCA-P 12.0 (Umetrics) for processing using PCA and PLS-DA (a regression extension of PCA used for supervised classification). Proton NMR data were Pareto scaled, in which each variable was centered and multiplied by $1/(S_k)^{1/2}$ where S_k is the s.d. of the variable.

Transgenic worms. The plasmids used in this study were generated using standard molecular biology techniques and Gateway technology (Invitrogen). All transgenic strains were generated by standard microinjection techniques[40].

Strains. The Bristol N2 strain was used as the wild type; worms were raised at 22 °C on NGM plates seeded with OP50 *E. coli*. All other strains generated for this work are listed in **Supplementary Table 1**.

39. Davis, M.W. *et al.* Rapid single nucleotide polymorphism mapping in *C. elegans*. *BMC Genomics* **6**, 118 (2005).
40. Mello, C.C., Kramer, J.M., Stinchcomb, D. & Ambros, V. Efficient gene transfer in *C. elegans*: extrachromosomal maintenance and integration of transforming sequences. *EMBO J.* **10**, 3959–3970 (1991).
41. Chen, B. *et al.* α-Catulin CTN-1 is required for BK channel subcellular localization in *C. elegans* body-wall muscle cells. *EMBO J.* **29**, 3184–3195 (2010).
42. Miller, K.G. *et al.* A genetic selection for *Caenorhabditis elegans* synaptic transmission mutants. *Proc. Natl. Acad. Sci. USA* **93**, 12593–12598 (1996).
43. Hammarlund, M., Davis, W.S. & Jorgensen, E.M. Mutations in β-spectrin disrupt axon outgrowth and sarcomere structure. *J. Cell Biol.* **149**, 931–942 (2000).
44. Fei, Y.J., Fujita, T., Lapp, D.F., Ganapathy, V. & Leibach, F.H. Two oligopeptide transporters from *Caenorhabditis elegans*: molecular cloning and functional expression. *Biochem. J.* **332**, 565–572 (1998).
45. Jiang, G. *et al.* A Na^+/Cl^--coupled GABA transporter, GAT-1, from *Caenorhabditis elegans*: structural and functional features, specific expression in GABA-ergic neurons, and involvement in muscle function. *J. Biol. Chem.* **280**, 2065–2077 (2005).
46. Fei, Y.-J. *et al.* Expression cloning of a mammalian proton-coupled oligopeptide transporter. *Nature* **368**, 563–566 (1994).
47. Beg, A.A. & Jorgensen, E.M. EXP-1 is an excitatory GABA-gated cation channel. *Nat. Neurosci.* **6**, 1145–1152 (2003).
48. Li, M.Z. & Elledge, S.J. Harnessing homologous recombination in vitro to generate recombinant DNA via SLIC. *Nat. Methods* **4**, 251–256 (2007).

doi:10.1038/nn.3575

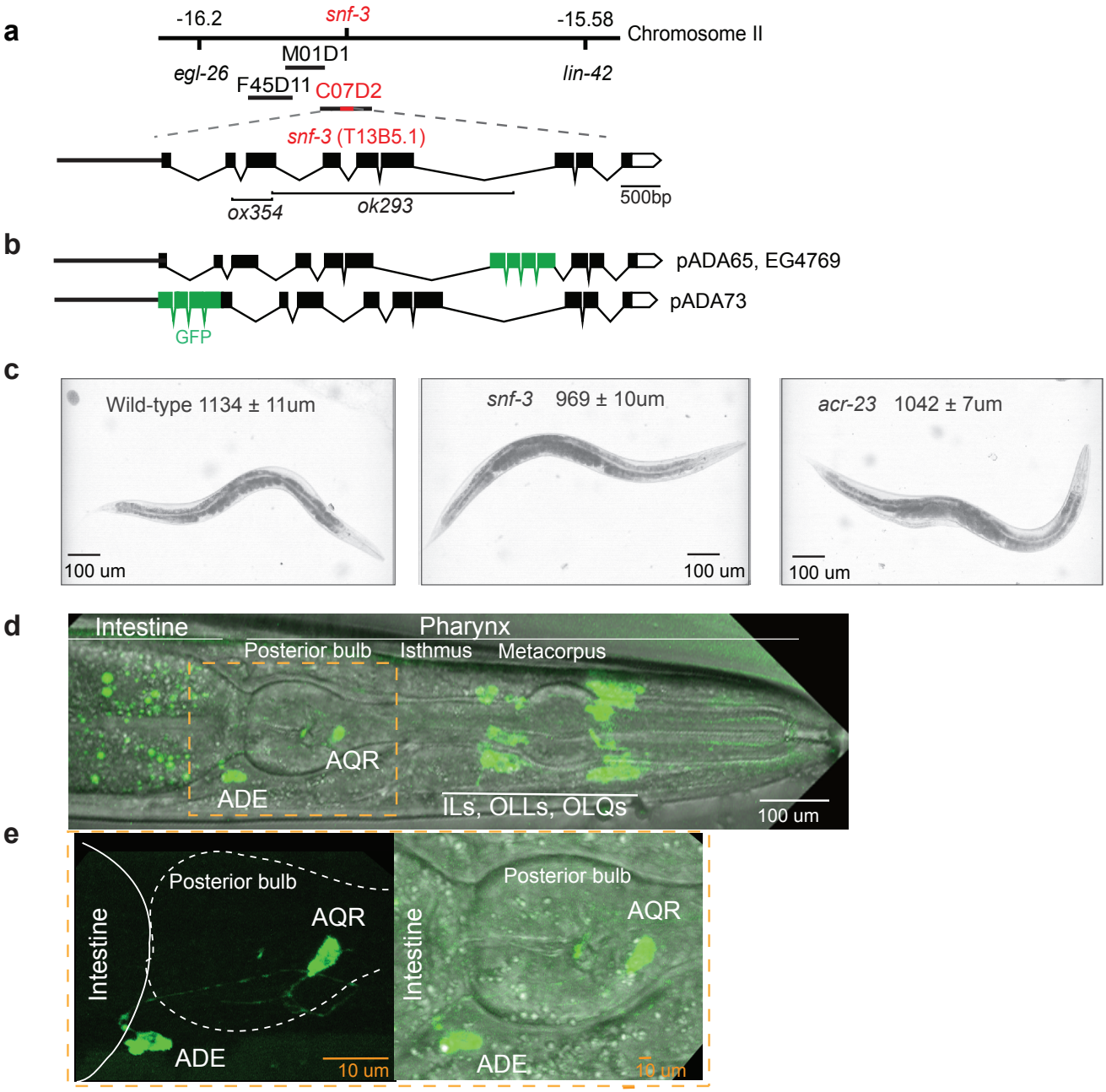

Supplementary Figure 1: *snf-3* gene and expression pattern.
(**a**) Genetic map and structure of the *snf-3* gene. The gene was identified by mapping *snf-3(ox354)* using single nucleotide polymorphisms and transgenic rescue. The *snf-3* locus maps to the left arm of chromosome II in a region covered by three cosmids, F45D11, M01D1 and C07D2. C07D2 and the gene T13B1.5 rescued the hypercontracted phenotype. T13B1.5 encodes the *snf-3* gene. *ox354* and *ok293* are deletion alleles. In *snf-3(ox354)* exons 2-3 are deleted, in *snf-3(ok293)* exons 3-6 are deleted. (**b**) pADA65 and pADA73 are the two SNF-3-GFP fusion plasmids used to determine SNF-3 expression and subcellular localization. EG4769 is a transgenic rescue strain injected with pADA65. (**c**) Representative images of adult hermaphrodites. *snf-3* and *acr-23* mutants alone are morphologically wild-type. *acr-23(-)* suppresses the *snf-3(-)* contribution to the *snf-3 egl-8* double mutant; that is, *acr-23 snf-3 egl-8* triple mutant resembles the *egl-8* single mutant. Values represent the mean length of a young adult animal for each genotype ± s.e.m. (**d**) SNF-3 is expressed in a limited set of neurons. The transgenic strain EG4769 carrying P*snf-3::SNF-3::GFP::snf-3*utr (also used in Figure 3a) was grown on RNAi against GFP to reveal neuronal expression. Neurons are resistant to the effects of RNAi. *snf-3*-expressing neurons in the head are the non-amphidial sensory neurons: 19 cell bodies around the metacarpus of the pharynx were identified as inner (ILs) and outer (OL) labial neurons based on cell body and dendrite positions. OLL= outer labial lateral, OLQ = outer labial quadrant. ADE was identified based on its position behind the posterior bulb of the pharynx, and AQR because this neuron is unilateral. * indicates unidentified neuron. (**e**) An enlargement of the posterior bulb region showing the morphology of the ADE and AQR neurons.

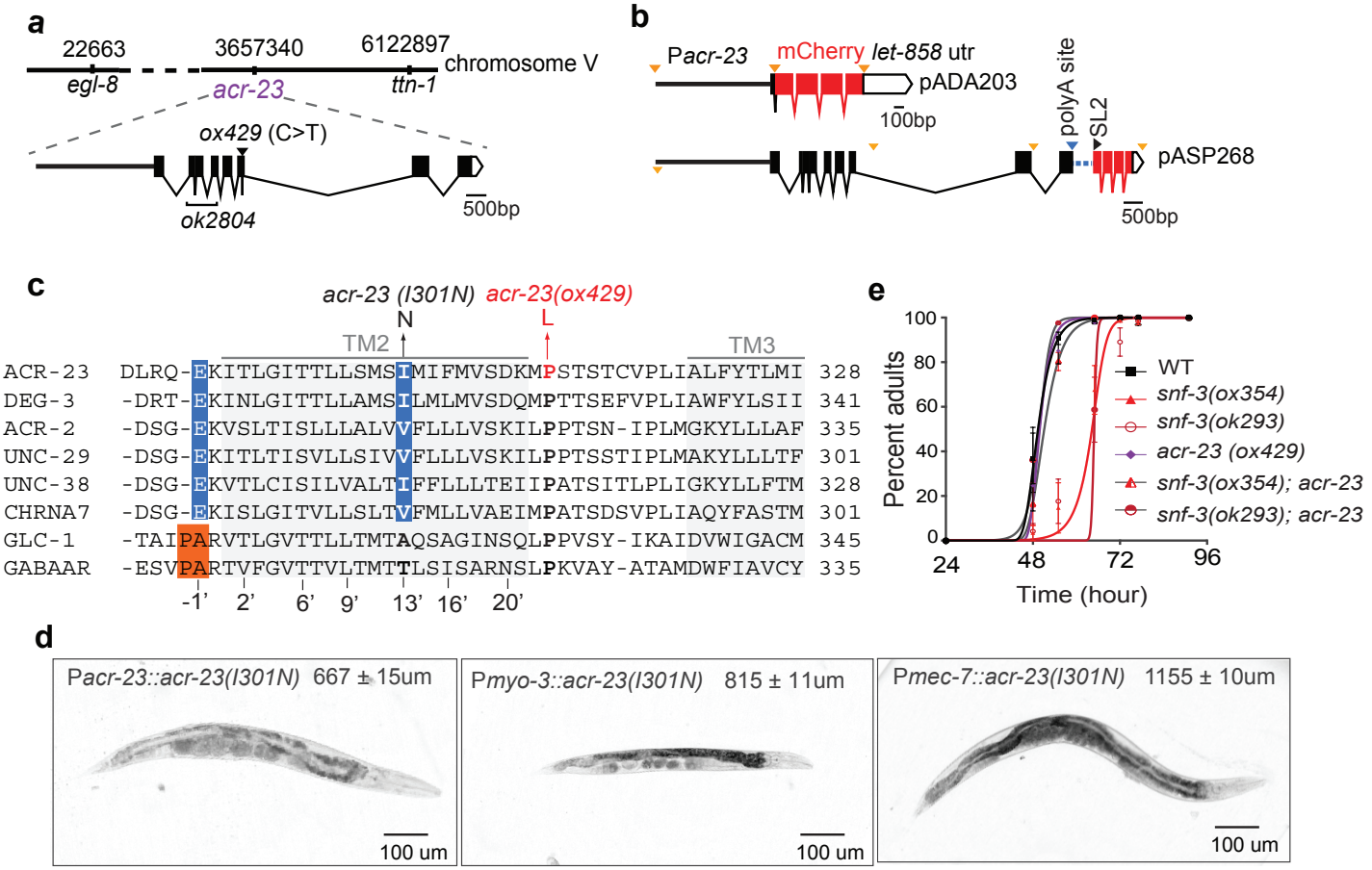

Supplementary Figure 2: The suppressor *ox429* is an allele of *acr-23.*
(a) *ox429* is an allele of *acr-23*, which encodes a cys-loop ligand-gated ion channel gene. The mutation *ox429* was identified using genome-wide Illumina sequencing of *snf-3 egl-8 ox429* triple mutant (EG6501). 448 single nucleotide polymorphisms (SNPs) were identified compared to the reference Bristol N2 genomic sequence. We found that 407 of these substitutions were either in non-coding sequences or were synonymous substitutions (silent changes at the amino acid level). We focused on the 41 SNPs with non-synonymous substitutions for further analysis. One SNP was contained in the *acr-23* gene, a nematode-specific cys-loop ligand-gated ion channel. The *ox429* is a C to T transition that causes the missense change P311L in the open reading frame. We confirmed that this change is the suppressor mutation by transgenic rescue and by crossing the null allele *acr-23(ok2804)* into the *snf-3 egl-8* double mutant. **(b)** pADA203 and pASP268 are transcriptional mCherry fusion plasmids used to determine the *acr-23* expression pattern. The yellow triangles denote Gateway (attB) recombination sites. For pASP268, we used the intergenic region of the *gpd-2 gpd-3* operon (dotted blue line) to express mCherry in an operon with the entire *acr-23* gene. The blue and black triangles denote the polyA site and the SL2 transplice acceptor site. **(c)** Alignment of the mutated region of ACR-23 with selected cys-loop ligand-gated ion channels. *C. elegans* AcetylCholine Receptor family member-23 (ACR-23; NP_504024.2); *C. elegans* Degeneration of certain neurons-3 (DEG-3; NP_505897.1); *C. elegans* AcetylCholine Receptor family member-2 (ACR-2; NP_509128.1); *C. elegans* UNCoordinated family member-29 (UNC-29; NP_492399.1); *C. elegans* UNCoordinated family member-38 (UNC-38; NP_491472.1); Human neuronal acetylcholine receptor subunit alpha-7 (CHRNA7; NP_001177384.1); *C. elegans* Glutamate-gated Chloride channel 1 (GLC-1; NP_507090.1); Human GABA-A alpha-1 (GABA-AR CAA32874.1). The residues that distinguish cation (blue) and anion (orange) selectivity for ligand-gated ion channels are highlighted. The C to T mutation in *ox429* converts a proline at position 311 to a leucine. This proline is conserved in all cys-loop ligand-gated channels and is required for receptor function (Deane CM *et. al.*, JBC, 2001). Mutations of the 13' position of the second transmembrane domain of two *C. elegans* receptors, *deg-3(u662)* (Treinin M *et. al.,* Neuron, 1995) and *acr-2(n2420)* (Jospin M *et. al.,* PloS Biol, 2009), cause a gain-of-function phenotype. We engineered an ACR-23 gain-of-function mutation based on the *deg-3(u662)* mutation in which an isoleucine was replaced by an asparagine (I301N). **(d)** Transgenic worms expressing an *acr-23(I301N)* gain-of-function receptor. P*myo-3* drives expression in body wall muscles. P*mec-7* drives expression in mechanosensory neurons. Behavioral analyses of these worms are shown in Figure 5 e-f. **(e)** *acr-23* suppresses *snf-3* growth defects. We measured the time from embryo to young adult. Egg-laying was synchronized by transferring parents to new plates every 6 hours. (mean of five independent assays ± s.e.m; *n*= 500 worms per experiment for each genotype). The data were fitted using KaleidaGraph 3.6 software.

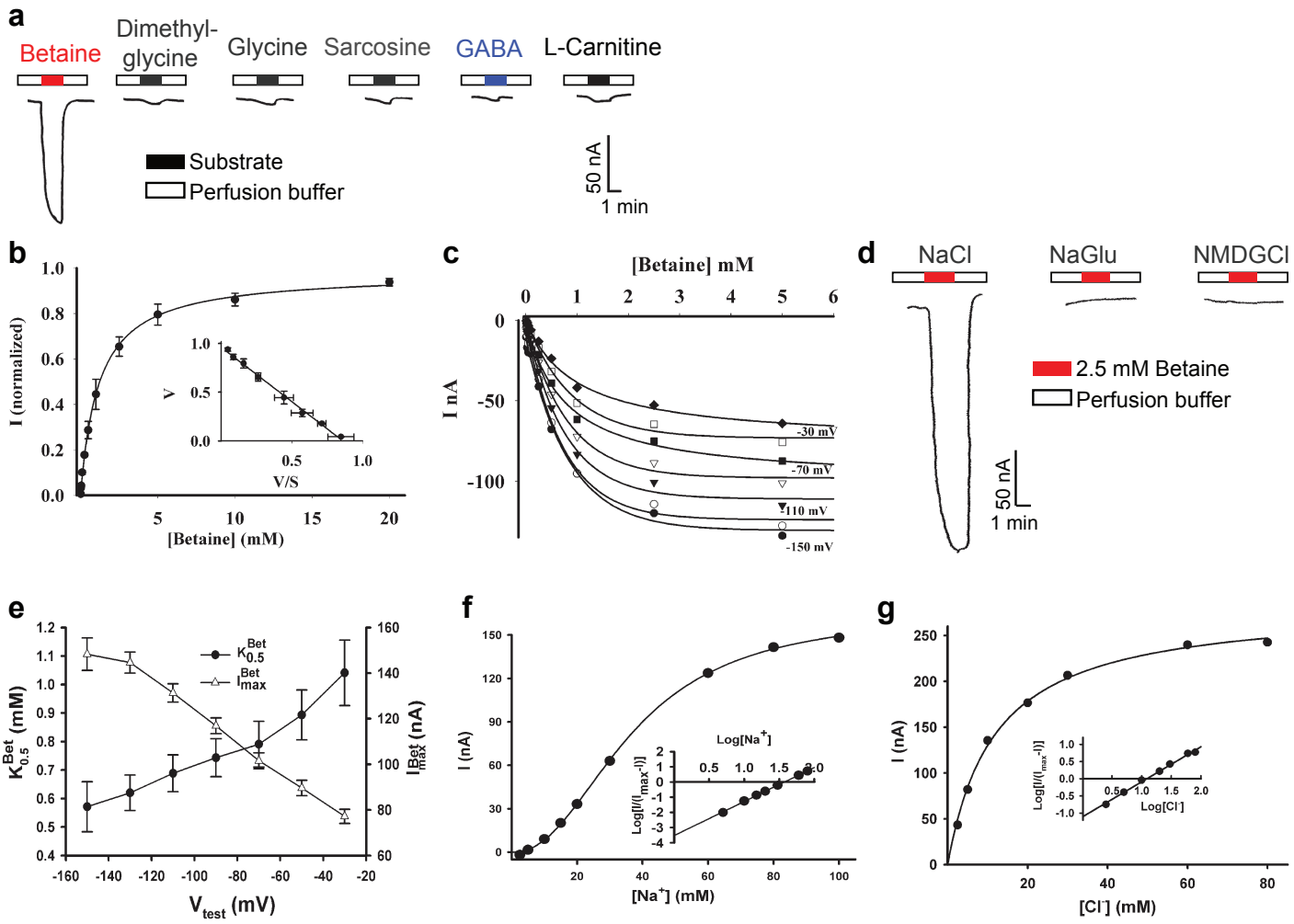

Supplementary Figure 3: SNF-3 transports betaine in *Xenopus* oocytes.
(**a**) Substrate specificity of SNF-3 in *Xenopus* oocytes. Representative current traces induced by 2.5 mM betaine, dimethylglycine (DM-glycine), glycine, sarcosine (methylglycine), GABA or L-carnitine in oocytes expressing SNF-3. **(b)** Saturation kinetics of SNF-3 activity. Betaine uptake conformed to Michaelis-Menten kinetics at each tested membrane potential (Inset: Eadie-Hofstee conversion of the same saturation data (v/s): [betaine uptake velocity (v) versus betaine uptake velocity/betaine concentration (v/s)). Betaine-induced currents were tested at a membrane potential of –50 mV and were normalized and fitted by non-linear regression (n=3 oocytes). Results are presented as mean ± SEM. **(c)** Betaine-induced currents are saturable over a range of membrane potentials. Representative recordings from each membrane potential tested. We used voltage steps to measure currents ranging from -30mV to -150mV. **(d)** SNF-3-mediated current is dependent on Na^+ and Cl^- ions. Chloride ions were replaced by gluconate (NaGlu), and sodium ions were replaced by N-methyl-D-glucamine (NMDGCl). **(e)** SNF-3 activity is regulated by membrane potential. Voltage-dependence of SNF-3 was determined by gradually changing membrane potential from –30 mV to –150 mV. The substrate-induced maximal current (I^{Bet}_{max}) increased from 77 ± 3 nA to 148 ± 7 nA and the Michaelis constant ($K^{Bet}_{0.5}$) changed from 1.0 ± 0.1 mM to 0.6 ± 0.1 mM. Kinetic parameters, $K_{0.5}$ and I_{max}, were determined at varying membrane potentials from three different oocytes after normalization. Results are presented as mean ± SEM. **(f,g)** Activation kinetics for SNF-3-mediated betaine transport by Na^+ **(f)** and Cl^- **(g)** Inset: Hill plot of SNF-3 affinities for Na^+ and Cl^- and their respective Hill coefficients (*h*) were determined at – 50 mV using the Hill equation. n= 3 oocytes for each ion. The Michaelis constant of SNF-3 for sodium ($K^{Na}_{0.5}$) was 37 ± 1 mM with a Hill coefficient of 2.2 ± 0.1, and the corresponding value for chloride ($K^{Cl}_{0.5}$) was 12 ± 1 mM with a Hill coefficient of 1.0 ± 0.1.

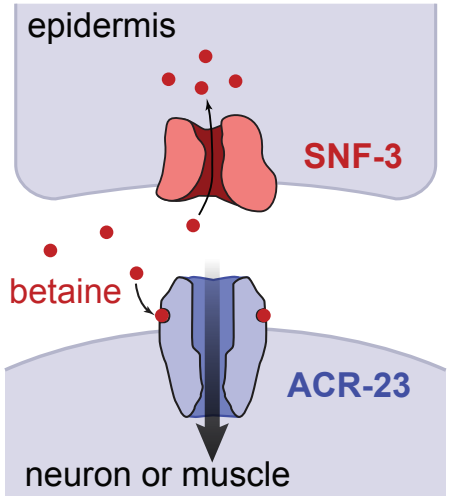

Supplementary Figure 4: A model for betaine function in *C. elegans.*
The SNF-3 transporter functions in the epidermis to limit betaine in the extracellular space.
The betaine receptor ACR-23 acts in a subset of neurons to regulate basal levels of locomotion.

Supplementary Table I: A list of all the strains that were generated for this work.

Strain name	Genotype
EG4085	*snf-3(ox354) II; egl-8(sa47) V; oxEx771[B0348(egl-8^{+}); rol-6(d);Pmyo-2::GFP]*
EG4094	*egl-8(sa47) V; oxEx771[B0348(egl-8^{+}); rol-6(sd); Pmyo-2::GFP]*
EG4769	*snf-3(ox354) II; egl-8(sa47) V; oxEx1067[snf-3::GFP(pPD114.24); Pmyo-2::mCherry; Punc-122::GFP]*
EG5005	*snf-3(ox354) II; egl-8(sa28) V*
EG5006	*snf-3(ox354) II; egl-8(n488) V*
EG5051	*snf-3(ox354) II ; egl-8(sa47) V; oxIs12[Punc-47:GFP, lin-15+] X; oxEx1208[Pdpy-30::snf-3::mCherry; Pmyo-2::mCherry]*
EG5052	*snf-3(ox354) II; egl-8(sa47) V; oxIs12[Punc-47::GFP, lin-15(+)] X; oxEx1209[Ppdi-2::snf-3::mCherry]*
EG5059	*snf-3(ox354) II; egl-8(sa47) V; oxIs12[Punc-47:GFP, lin-15+] X; oxEx1219[Prab-3::egl-8-mCherry; Pmyo-2::GFP; ladder]*
EG5060	*snf-3(ox354) II; egl-8(sa47) V; oxIs12[Punc-47:GFP; lin-15+] X; oxEx1220[Pdpy-30::egl-8-mcherry; Pmyo-2::GFP; ladder]*
EG5124	*snf-3(ok293) II; egl-8(sa47) V*
EG5485	*unc-22(ox431) IV*
EG6315	*snf-3(ok293) II* from RM2716 outcrossed twice against N2
EG6326	*acr-23(ox429) V*
EG6327	*snf-3(ox354) II; acr-23(ox429) V*
EG6328	*snf-3(ox354) II; acr-23(ok2804) V*
EG6544	*snf-3(ox354) II; egl-8(sa47) V; acr-23(ok2804) V*
EG6566	*acr-23(ox429) V*
EG6785	*lin-15(n765ts) X; oxEx1595[acr-23(I301N); lin-15(+)]*
EG6786	*lin-15(n765ts) X; oxEx1596[acr-23(I301N); lin-15(+)]*
EG6879	*snf-3(ox354) II; egl-8(sa47) V; oxIs12[Punc-47::GFP; lin-15(+)]X; oxEx1179[Pvha-6::snf-3::mCherry]*
EG6881	*snf-3(ox354) II; egl-8(sa47) V; oxIs12[Punc-47::GFP; lin-15(+)] X; oxEx1246[Podr-4::snf-3::mCherry]*
EG6882	*snf-3(ox354) II; egl-8(sa47) V; oxIs12[Punc-47::GFP; lin-15(+)] X; oxEx1245[Punc-17::snf-3::mCherry]*
EG6885	*snf-3(ox354) II* outcrossed seven times against N2
EG6887	*snf-3(ox354) II; egl-8(sa47) V*
EG6888	*lin-15(n765ts) X; oxEx1614[Psnf-3::GFP::snf-3::let-858; lin-15(+); Pmyo-2::mCherry; Punc-122::GFP]*
EG6958	*snf-3(ox354) II; egl-8(sa47) V; oxIs12[Punc-47::GFP; lin-15(+)] X; oxEx1618[Pgtl-3::snf-3::mCherry]*
EG6957	*snf-3(ox354) II; egl-8(sa47) V; oxIs12[Punc-47::GFP; lin-15(+)] X; oxEx1617[Psnf-3::snf-3::mCherry]*
EG7080	*snf-3(ok293) II; acr-23(ox429) V*
EG7081	*snf-3(ox354) II; egl-8(sa47) V* outcrossed 4 times against N2
EG7083	*unc-54(e190) I; snf-3(ox354) II; egl-8(sa47) V*
EG7084	*unc-54(e1092) I; snf-3(ox354) II; egl-8(sa47) V*
EG7345	*lin-15(n765ts) X; oxEx1790[Pmyo-3::acr-23(I301N); lin-15(+)]*
EG7346	*lin-15(n765ts) X; oxEx1791[Pmyo-3::acr-23(I301N); lin-15(+)]*
EG7347	*lin-15(n765ts) X; oxEx1792[Pmec-7::acr-23(I301N); lin-15(+)]*
EG7348	*lin-15(n765ts) X; oxEx1793[Pmec-7::acr-23(I301N); lin-15(+)]*

EG7416	*lin-15(n765ts) X; oxEx1790[Pacr-23::mCherry::let-858; lin-15(+); Pmyo-2::GFP]*
EG7513	*snf-3(ox354) II; egl-8(sa47) V* outcrossed 11 times against N2
EG7681	*snf-3(ox354) II; egl-8(sa47) V; oxIs12[Punc-47::GFP; lin-15(+)] X; oxEx1219[Prab-3::egl-8-mCherry; Pmyo-2::GFP; ladder]*
EG7682	*snf-3(ox354) II; egl-8(sa47) V; oxIs12[Punc-47::GFP; lin-15(+)] X; oxEx1236[Pdpy-7::egl-8cDNA::mCherry; Pmyo-2::GFP]*
EG7685	*snf-3(ox354) II; egl-8(sa47) V; oxEx1906[Pvha-6::egl-8::mCherry; Pmyo2::GFP]*
EG7686	*snf-3(ox354) II; egl-8(sa47) V; oxEx1906[Pvha-6::egl-8::mCherry; Pmyo2::GFP]*
EG7710	*acr-23(ok2804) V* from RB2119 outcrossed 4 times against N2
EG7711	*snf-3(ox354) II; egl-8(sa47) V; oxEx1909[Punc-17::egl-8::mCherry; Pmyo-2::GFP]*
EG7712	*snf-3(ox354) II; egl-8(sa47) V; oxEx1909[Punc-17::egl-8::mCherry; Pmyo-2::GFP]*
EG8006	*snf-3(ox354) II; egl-8(sa47) V; oxEx1925[Pvit-2::snf-3::mCherry; Pmyo-2::GFP]*
EG8007	*snf-3(ox354) II; egl-8(sa47) V; oxEx1925[Pvit-2::snf-3::mCherry; Pmyo-2::GFP]*
EG8033	*egl-8(sa47) V* outcrossed 10 times against N2
EG8093	*oxEx1208[Pdpy-30::snf-3::mCherry; Pmyo-2::mCherry]*
EG8095	*acr-23(ox429) V* outcrossed 4 times against N2
EG8099	*acr-23(ox429) V; oxEx1959[Pacr-23::acr-23::acr-23 3'utr; Pmyo-2::GFP]*
EG8100	*acr-23(ox429) V; oxEx1959[Pacr-23::acr-23::acr-23 3'utr; Pmyo-2::GFP])*
EG8103	*acr-23(ox429) V; oxEx1962[Pmec-7::acr-23::let-858utr; Pmyo-2::mCherry; Punc-122::mCherry]*
EG8105	*acr-23(ox429) V; oxEx1962[Pmec-7::acr-23::let-858utr; Pmyo-2::mCherry; Punc-122::mCherry]*
EG8106	*acr-23(ox429) V; oxEx1965[Prab-3::acr-23-gfp::let-858utr; Pmyo-2::mCherry]*
EG8108	*acr-23(ox429) V; oxEx1965[Prab-3::acr-23-gfp::let-858utr; Pmyo-2::mCherry]*
EG8109	*acr-23(ox429) V; oxEx1969[Pmyo-3::acr-23::GFP::let-858utr; Pmyo-2::mCherry]*
EG8110	*acr-23(ox429) V; oxEx1969[Pmyo-3::acr-23::GFP::let-858utr; Pmyo-2::mCherry]*
JT47	*egl-8(sa47) V*
RB2119	*acr-23(ok2804) V*
RM2716	*snf-3(ok293) II; dpy-11(e224) V*